POLITECNICO DI TORINO
I Facoltá di Ingegneria
Corso di Laurea in Ingegneria Matematica

Tesi di laurea specialistica

Collective Behaviour of three-dimensional linear perturbation waves in shear flow

Autore:
Marco Mastinu

Relatore:
Prof. D. Tordella

Corelatore:
Dott. S. Scarsoglio

Luglio 2011

Contents

List of Figures

Chapter 1

Introduction

The concept of collective behaviour for ensembles of physical and biological entities is common practice in science. In hydrodynamics, it is almost confined into the context of turbulent systems. This work, propose to export it into the framework of small perturbation dynamics of stable and unstable flows.

With the aim to understand whether the nonlinear interaction among different scales in fully developed turbulence can affect the energy spectrum, and to quantify the level of generality on the value of the energy decay exponent of the inertial range, is considered the state that precedes the onset of instability and transition to turbulence. In this condition, the system is constituted by multiple spatial and temporal scales, and is subject to all the processes of the linearized perturbative Navier-Stokes equations: linearized convective transport, linearized vortical stretching, and molecular diffusion. With the important exception of the nonlinear interaction, these features are the same as those characterizing the turbulent state. The linear transient dynamics of three-dimensional perturbations, which is governed by the initial-value problem related to the linearized perturbative Navier-Stokes equations, is very complicated and shows a great variety of different behaviours, not a priori predictable.

We ask whether the linearized perturbative system is able to show a power-law scaling for the energy spectrum in an analogous way to the Kolmogorov argument. It is determined the decay exponent of the energy spectrum for arbitrary longitudinal and transversal perturbations acting on a typical shear flow i.e. the bluff-body wake. Then, the energy spectrum of the linearized perturbative system is compared with the well-known $-5/3$ Kolmogorov power-law scaling. It is observed, for both longitudinal and transversal perturbative waves, a decay rate of $-5/3$ in the intermediate range ($2 < k < 100$), while the energy decays more rapidly for Iarger

wavenumbers ($k > 100$). So far, it seems that the nonlinear interaction is not the main factor responsible of the specific value of the $-5/3$ decay exponent in the energy spectrum and the spectral power-law scaling of inertial waves is a general dynamical property of the Navier-Stokes equations, valid also for a general small perturbation which lives in the linearized system.

Chapter 2

Stability and turbulence

2.1 Introduction

In this chapter the concepts of stability and turbulence are introduced. A flow is said instable if spontaneously changes to one type of motion to another. The central notion is that a configuration is unstable when small perturbations to it tend to be amplified. Hydrodynamic stability concerns the stability and instability of fluids. The concept of stability of a state of a physical or mathematical system was understood in the eighteen century, and Clerk Maxwell (see Betchov & Criminale, (1967)) expressed the qualitative concept clearly in the nineteenth. Hydrodynamic stability is an importan part of fluid mechanics, because an unstable flow is not observable, an unstable flow being in practice broken down rapidly by some "small variation" or another. Also unstable flows often evolve into an important state of motion called turbulence.

Turbulence is a omnipresent phenomenon of Nature. In our everyday life, we either rarely notice it when swimming, driving a car, riding a bike, skating, or suddenly pay serious attention to it, when the ride gets bumpy on board a plane on stormy weather or when flying over tall mountains. Actually, the diversity of situations where we discover turbulence as an important scientific phenomenon is impressive: flow around ships and aircrafts, combustion in car engines and plane turbines, flow in the ocean, atmosphere, air flow in lungs, flow of blood in arteries and heart, flow in pipelines, even the dynamics of the financial markets can also be viewed as analogous to turbulent flows. The entire Universe appears to be in a state of turbulent motion, and turbulence seems to be a decisive factor helping in the formation of stars and solar systems, as indicated by astronomical observations and theoretical considerations in astrophysics. From the large variety of sit-

uations mentioned above, many of them are cases in which turbulence is attractive from the point of view of the engineer, since studying it leads to technological improvement. It is more fruitful then to model regions where the turbulent flows interact with boundaries, and then learn how to control and apply them. For the physicist, the interesting part is how the small-scale structure of turbulence is organized, preferably isolated from any boundary effects. This is where universal aspects can be sought, in the sense that they should be independent of the nature of the fluid or the geometry of the problem. It is universality that makes turbulence an exciting research subject for physicistsand mathematicians.

2.2 Stability definition

In examining the dynamics of any physical system the concept of stability becomes relevant only after first enstablishing the possibility of equilibrium. Once this step has been taken, the concept become ubiquitous, regardless of he actual system being probed. As expressed by [4], stability can be defined as *the ability of a dynamical system to be immune to small disturbances.* It is clear that the disturbances need not necessarily be small in magnitude but the fact that the disturbances become amplified as a resuts and then is a departure from any state of equilibrium tha system had is implicit. In this work the attention is focused on hydrodynamical stability of incompressible flows. For this kind of flows evolutive equations are

$$\nabla \cdot \mathbf{u} = 0, \tag{2.1}$$

$$\rho \left(\frac{\partial \mathbf{u}}{\partial t} + \mathbf{u} \cdot \nabla \mathbf{u} \right) = -\nabla \mathbf{p} + \mu \nabla^2 \mathbf{u} + \mathbf{F}, \tag{2.2}$$

where $\mathbf{u}(\mathbf{x}, t)$ is the velocity field, $\mathbf{p}(\mathbf{x}, t)$ is the pressure field, $\mathbf{F}(\mathbf{x}, t)$ is the external force field, ρ is the mass density and μ is kinematic viscosity. Equation (2.1) is the continuity equation and express the incompressibility property of the flow, while (2.2) is the Newton law. Equation (2.2) is also known as the Navier-Stokes equation. Defining U and L as the characteristic velocity and length scales of the flow, and ν the kinematic viscosity, an adimensionalizations of (2.2) can be made. The adimensionalized Navier-Stokes equation depends only on one parameter, the Reynols number Re

$$Re = \frac{\rho U l}{\mu} = \frac{U l}{\nu}, \tag{2.3}$$

The Reynolds number may be interpreted as the ratio of inertial to viscous forces present in the fluid, and for an incompressible flow, it is the only control parameter of that system.

Hydrodynamic stability theory is concerned with the response of a laminar flow to a disturbance of small or moderate amplitude. If the flow returns to its original laminar state one defines the flow *stable*, whereas if the disturbance grows and causes the laminar flow to change into a different state one defines the flow *unstable*. Instabilities often results in *turbulence* fluid motion, but they may also take the flow into a different laminar, usually more complicated state. Stability theory deals with the mathematical analysis of evolution of disturbances superposed on a laminar *base flow*. In many cases one assumes that the disturbances to be *small* so that further simplifications can be justified. In particular, a linear equation governing the evolution of disturbances is desirable. As the disturbance velocities grow above a few percent of the base flow, nonlinear effects become important and the linear equations no longer accurately predict the disturbance evolution. Although the linear equations have limited region of validity they are important in detecting physical grow mechanisms and identifying dominant disturbance type.

2.3 Turbulence

Skipping over the dictionary definition, which does not suffice to characterize the modern physical sense of the word, we stop at the definition given in 1937 by Taylor and Von Karman: *Turbulence is an irregular motion which in general makes its appearance in fluids, gaseous or liquid, when they flow past solid surfaces or even when neighboring streams of the same fluid past or over one another.* To make this more clear, we need to use the terminology of fluid dynamics. Flows of gases and liquids can be divided into two very different types: *laminar* flows, which are smooth and regular, and *turbulent*, totally opposite, in which physical quantities as velocity, temperature, pressure, etc. fluctuate in a sharp and irregular manner in space and time, the latter being actually the more natural state of a flow.

In section (2.2) it is explained that unstable flows evolve towards *turbulence*. Each time a flow changes as a results of an instability, one's ability to predict the details of the motion is reduced. When successive instabilities have reduced the level of predictability so much that it is appropriate to describe a flow statistically, rather than in every detail, than one says that the flow is turbulent. This implies that random features of the flow are dominant. One cannot, however, say that a turbulent flow is completly

random, because this is like to say that turbulence does not exist. All flows involve in organized structures, so the point is just whether the randomness is sufficient for statistical description to be most appropriate. There is every reason to suppose that the loss of predictability occurs as a property of the Navier-Stokes equation (2.2) and not because these equations are no more able to describe the physical system.

2.4 Statistical description of turbulence

In principle, the phenomenology of turbulence is characterized by simple statistical quantities, such as averages, probability distribution functions, spectra, correlations, etc., which are calculated from data experimentally measured or from direct computer simulations. In general, the term "averaging" is never equivalent to a proper ensemble average (over all possible states of the system), but ergodicity is invoked to replace it by time-averaging or mixed time and limited spatial averaging. These tools are sufficient to reveal some of the most important universal features of turbulence.

2.5 Turbulence hierarchy and energy cascade

Based on the technological interest raised by the remarkable momentum transfer properties of the large scales of turbulence, experiments in the beginning of the 20th century led to decisive advances in the theory of turbulence. Representative of this time are the so-called semi-empirical approaches made by great fluid-dynamicists, such as G. Taylor, L. Prandtl and T. Von Karman in the 1920s and '30s, which were used to solve important practical problems. In a remarkable paper, Lewis Fry Richardson advanced in 1922 the assumption that turbulence is organized as an hierarchy of eddies of various scales, each generation borrowing energy from its immediately larger neighbor in a "cascade" process of eddy-breakdown [2]. Richardson's notion of turbulence was that a turbulent flow is composed by "eddies" of different sizes. The sizes define a characteristic length scale λ for the eddies, which are also characterized by velocity scales v_λ and time scales t_λ (turnover time) dependent on the length scale. The large eddies are unstable and eventually break up originating smaller eddies, and the kinetic energy of the initial large eddy is divided into the smaller eddies that stemmed from it. These smaller eddies undergo the same process, giving rise to even smaller eddies which inherit the energy of their predecessor eddy, and so on. In this way, the energy is passed down from the large scales L of the motion to smaller scales λ until

reaching a sufficiently small length scale λ_0 such that the viscosity of the fluid can effectively dissipate the kinetic energy into internal energy. This picture, though more appropriate in wavenumber space (where the wavenumber k corresponding to length scale λ is $k = 2\pi/\lambda$), was poetically immortalized in his book inspired from observation of clouds and the verses of Jonathan Swift: *Big whorls have little whorls, which feed on their velocity; and little whorls have lesser whorls, and so on to viscosity (in the molecular sense).* This era culminated with the now fundamental ideas of Andrei Nikolaevich Kolmogorov in the *theory of locally isotropic turbulence* (1941) [3].

2.6 Isotropic homogeneous turbulence

Inspired by Richardson's energy cascade description, shown in figure (2.1), Kolmogorov assumed that with each step in the energy transfer towards smaller scales, the anisotropic influence of the large scales will gradually be lost, such that at sufficiently small scales the flow will be *statistically homogeneous and isotropic.* In his original theory of 1941, Kolmogorov postulated that for very high Reynolds number, the small scale turbulent motions are statistically isotropic (i.e. no preferential spatial direction could be discerned). In general, the large scales of a flow are not isotropic, since they are determined by the particular geometrical features of the boundaries. This steady situation, characterized by a mean flux of energy ε, was postulated by Kolmogorov to be universal and determined by only one parameter.

Moving further down the scales (i.e. increasing wavenumber k), there comes a length-scale λ_0 where the flow gradients are so large that viscous effects can no longer be ignored. So, for very high Reynolds numbers the statistics of small scales are universally and uniquely determined by the viscosity ν and the rate of energy dissipation ε. With only these two parameters, the unique length that can be formed by dimensional analysis is

$$\lambda_0 = \left(\frac{\nu^3}{\varepsilon}\right)^{1/4} \tag{2.4}$$

Below the famous self-similarity hypotheses in their original form are introduced (according to Hinze [4]):

1. At sufficiently large Reynolds numbers there is a range of high wave numbers k (inertial-range) where the turbulence is statistically in equilibrium and uniquely determined by the parameters ε and ν. This state of equilibrium is universal.

2. If the Reynolds number is infinitely large, the energy spectrum in the inertial range is independent of ν and solely determined by the parameter ε.

Dissipation of kinetic energy takes place at scales of the order of Kolmogorov length λ_0, while the input of energy into the cascade comes from the decay of the large scales, of order L. These two scales at the extremes of the cascade can differ by several orders of magnitude at high Reynolds numbers. In between there is a range of scales (each one with its own characteristic length λ) that has formed at the expense of the energy of the large ones. These scales are very large compared with the Kolmogorov length, but still very small compared with the large scale of the flow (i.e. $\lambda_0 << \lambda << L$). Since eddies in this range are much larger than the dissipative eddies that exist at Kolmogorov scales, kinetic energy is essentially not dissipated in this range, and it is merely transferred to smaller scales until viscous effects become important as the order of the Kolmogorov scale is approached. Within this range inertial effects are still much larger than viscous effects, and it is possible to assume that viscosity does not play a role in their internal dynamics (for this reason this range is called "inertial range").

By small scales we will understand the dissipative range close to λ_0 and the inertial range postulated by the first Kolmogorov hypothesis (1). Phenomenological studies of turbulence are mostly aimed at the study of the small scales, since it is here that universal properties of turbulence are seen, and their characterization is considered important for the *turbulence problem*. The second hypothesis of Kolmogorov (2) implies that small-scale (high wavenumbers k) turbulence is isotropic and homogeneous at sufficiently large Reynolds numbers, and its statistics will be determined only by the average dissipation rate

$$\varepsilon = \frac{\nu}{2} \left\langle \left(\frac{\partial u_i}{\partial x_j} + \frac{\partial u_j}{\partial x_i} \right)^2 \right\rangle, \tag{2.5}$$

where ν is the flow viscosity.

The way in which the kinetic energy is distributed over the multiplicity of scales is a fundamental characterization of a turbulent flow. For homogeneous turbulence (i.e., statistically invariant under translations of the reference frame) this is usually done by means of the energy spectrum function $E(k)$, where k is the modulus of the wavevector corresponding to some harmonics in a Fourier representation of the flow velocity field $\mathbf{u}(\mathbf{x})$

$$\mathbf{u}(\mathbf{x}) = \iiint_{\mathbb{R}^3} \hat{\mathbf{u}}(\mathbf{k}) e^{i\mathbf{k}\cdot\mathbf{x}} d^3\mathbf{k}, \tag{2.6}$$

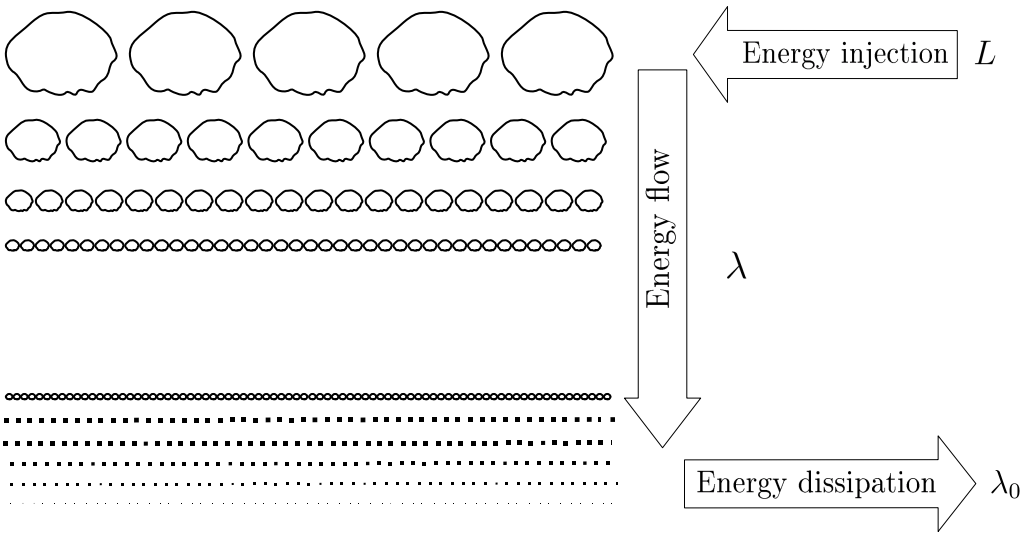

Figure 2.1: Richardson energy cascade. Process of eddy-breakdown: larger eddys (external scale L) split into smaller eddys (inertial scale λ). Energy transfer occur from bigger to smaller eddys since the dissipation scale (scale λ_0) is reached. Scale λ_0 is defined as the scale where inertial and dissipation effects are of the same order of magnitude.

where $\hat{\mathbf{u}}(\mathbf{k})$ is the Fourier transform of the velocity field. Thus, $E(k)dk$ represents the contribution to the kinetic energy from all the Fourier modes with $k < |\mathbf{k}| < k + dk$, and therefore,

$$E_{tot} = \int_0^\infty E(k)dk. \tag{2.7}$$

According with the (1) hypothesis, the spectrum function of energy E is indipendent of the energy production process for all wavenumbers large compared with those at which the production occurs. Then E depends only on the wavenumber, the dissipation, and viscosity,

$$E = E(k, \varepsilon, \nu). \tag{2.8}$$

If the cascade is long enough, there may be an intermediate range (the inertial range) in which the action of viscosity has not yet come in, that is

$$E = E(k, \varepsilon). \tag{2.9}$$

Thus if the form $E(k, \varepsilon) = C\,\varepsilon^\alpha k^\beta$ is supposed, by dimension analysis

$$E = C\,\varepsilon^{2/3} k^{-5/3}, \tag{2.10}$$

where C would be a universal constant. This is one of the most famous results of Kolmogorov 1941 theory (the $-5/3$ power-law), and considerable experimental evidence has accumulated that supports it [15]. In figure (2.2) is shown the energy spectrum.

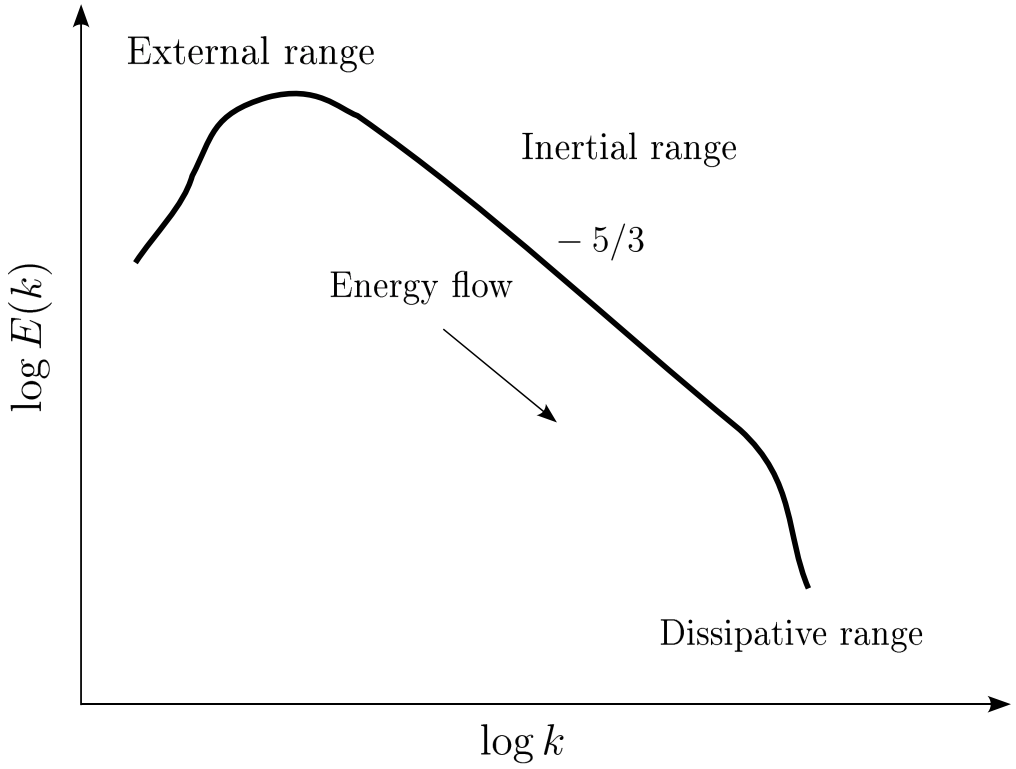

Figure 2.2: Energy spectrum.

Chapter 3

The Normal Mode Stability Theory

In this chapter the linear stability analysis is introduced and carried on through the classical modal treatment. The essentials of the normal mode theory are presented for three-dimensional viscous incompressible steady parallel flows. After the perturbed system is introduced and the resulting equations are linearized, a partial differential equation is obtained to describe the spatio-temporal evolution of the perturbation (see section 3.2). The normal mode theory is presented and, subsequently, the Orr-Sommerfeld equation is derived by introducing the stability characteristics section 3.3. The dispersion relation is defined and the concepts of convective and absolute instability are discussed in section 3.6.

3.1 Introduction

Traditionally, investigations of disturbances in shear flows have been characterized using classical linear stability analysis. This concept is well founded and is, in principle, correctly recognized as an initial-value problem. However, instead of considering the complete temporal evolution of the perturbations and analyzing the physical cause of a possible instability, the attention has been widely focused on determining whether or not the flow is asymptotically unstable. If only the question of stability is to be answered, the modal analysis turns out to be a powerful and synthetic means. First contributions have been given by [24], [25] and [30] who separately derived the now-famous Orr-Sommerfeld equation. More recently, significant results in literature for the bluff-body wake stability have been offered by, among others, [23], [33], [20], [18]. The modal theory to study the stability of the flow is based on

the perturbative analysis. Once the base flow is known, small oscillations are imposed and their asymptotic fate is considered. If they are damped the flow is stable, while if they are amplified the flow is unstable. In the framework of the modal analysis, the solution of the linearized perturbative equations turns into the resolution of an eigenvalue problem, the Orr-Sommerfeld equation.

3.2 Perturbed flow and linearized disturbance equations

It is now assumed the base flow to be steady, parallel, incompressible and viscous. It is described by the physical quantity

$$\vec{U}(t,x,y,z) = \begin{cases} u(t,x,y,z) = U(y), \\ v(t,x,y,z) = 0, \\ w(t,x,y,z) = 0, \\ p(t,x,y,z) = P(x). \end{cases}$$

The perturbed flow can be decomposed into a steady part and a fluctuating component that oscillates about the base flow

$$\vec{u}(t,x,y,z) = \begin{cases} u(t,x,y,z) = U(y) + \tilde{u}(t,x,y,z), \\ v(t,x,y,z) = \tilde{v}(t,x,y,z), \\ w(t,x,y,z) = \tilde{w}(t,x,y,z), \\ p(t,x,y,z) = P(x) + \tilde{p}(t,x,y,z). \end{cases}$$

where the widetilde superscripts indicate fluctuation components that are small with respect to the corresponding mean system quantities

$$|\tilde{u}/U| << 1, \quad |\tilde{v}/U| << 1, \quad |\tilde{w}/U| << 1, \quad |\tilde{p}/P| << 1.$$

By writing the continuity and the Navier-Stokes equations for the perturbed flow and then subtracting from these the corresponding ones for the base flow, one obtains the following

$$\begin{cases} \dfrac{\partial \tilde{u}}{\partial x} + \dfrac{\partial \tilde{v}}{\partial y} + \dfrac{\partial \tilde{w}}{\partial z} = 0, \\ \dfrac{\partial \tilde{u}}{\partial t} + U\dfrac{\partial \tilde{u}}{\partial x} + \tilde{u}\dfrac{\partial \tilde{u}}{\partial x} + \tilde{v}U' + \tilde{u}\dfrac{\partial \tilde{u}}{\partial y} + \tilde{w}\dfrac{\partial \tilde{u}}{\partial z} + \dfrac{\partial \tilde{p}}{\partial x} = \dfrac{1}{Re}\nabla^2\tilde{u}, \\ \dfrac{\partial \tilde{v}}{\partial t} + U\dfrac{\partial \tilde{v}}{\partial x} + \tilde{u}\dfrac{\partial \tilde{v}}{\partial x} + \tilde{v}\dfrac{\partial \tilde{v}}{\partial y} + \tilde{w}\dfrac{\partial \tilde{v}}{\partial z} + \dfrac{\partial \tilde{p}}{\partial y} = \dfrac{1}{Re}\nabla^2\tilde{v}, \\ \dfrac{\partial \tilde{w}}{\partial t} + U\dfrac{\partial \tilde{w}}{\partial x} + \tilde{u}\dfrac{\partial \tilde{w}}{\partial x} + \tilde{v}\dfrac{\partial \tilde{w}}{\partial y} + \tilde{w}\dfrac{\partial \tilde{w}}{\partial z} + \dfrac{\partial \tilde{p}}{\partial z} = \dfrac{1}{Re}\nabla^2\tilde{w}. \end{cases} \tag{3.1}$$

The system of equations (3.1) is non-linear with respect to the disturbance terms. The non-linear terms are products of the fluctuating velocities and their derivatives. If the oscillation has frequency ω, these terms will have frequency 0 o 2ω. This interaction will either modify the base flow (mean-flow distortion) and feedback to the fluctuating components or introduce higher harmonics. Such difficulties are overcame if it is assumed that the products of the fluctuations and their derivatives have small amplitudes. The terms

$$\begin{gathered} \tilde{u}\frac{\partial \tilde{u}}{\partial x}, \quad \tilde{v}\frac{\partial \tilde{u}}{\partial y}, \quad \tilde{w}\frac{\partial \tilde{u}}{\partial z}, \\ \tilde{u}\frac{\partial \tilde{v}}{\partial x}, \quad \tilde{v}\frac{\partial \tilde{v}}{\partial y}, \quad \tilde{w}\frac{\partial \tilde{v}}{\partial z}, \\ \tilde{u}\frac{\partial \tilde{w}}{\partial x}, \quad \tilde{v}\frac{\partial \tilde{w}}{\partial y}, \quad \tilde{w}\frac{\partial \tilde{w}}{\partial z}, \end{gathered}$$

are negligible in comparison with the other terms as a small disturbance multiplied by a small disturbance results in a term of smaller order of magnitude and no longer influences the equations to this order of approximation. The linear system is

$$\begin{cases} \dfrac{\partial \tilde{u}}{\partial x} + \dfrac{\partial \tilde{v}}{\partial y} + \dfrac{\partial \tilde{w}}{\partial z} = 0, \\ \dfrac{\partial \tilde{u}}{\partial t} + U\dfrac{\partial \tilde{u}}{\partial x} + \tilde{v}U' + \dfrac{\partial \tilde{p}}{\partial x} = \dfrac{1}{Re}\nabla^2\tilde{u}, \\ \dfrac{\partial \tilde{v}}{\partial t} + U\dfrac{\partial \tilde{v}}{\partial x} + \dfrac{\partial \tilde{p}}{\partial y} = \dfrac{1}{Re}\nabla^2\tilde{v}, \\ \dfrac{\partial \tilde{w}}{\partial t} + U\dfrac{\partial \tilde{w}}{\partial x} + \dfrac{\partial \tilde{p}}{\partial z} = \dfrac{1}{Re}\nabla^2\tilde{w}. \end{cases} \tag{3.2}$$

The perturbations applied to the system will evolve independently because the nonlinear terms, that would permit interaction, have been neglected. The same fundamental property of linearity occurs in other fields (acoustics, electromagnetism, ...), but non-linear equations must often be retained to capture the essential physics. Luckily, the solution of the linear system is sufficient to describe problems where small oscillations influence the base flow. Moreover, it should be reminded that the infinitesimal perturbations cannot be removed and are always present in any physical system. Due to the assumption of small disturbances, the solution of the original problem can be approximated with the one of the linear system. However, as soon as the perturbation energy grows, the non-linear equations are required to correctly capture the perturbative evolution. For this reason, only the onset (and not the following temporal evolution) of a possible instability is the aim of the linear stability theory.

3.3 Normal mode hypothesis and Orr-Sommerfeld equation

The linearity of the system is immediately exploited by seeking solutions in terms of complex functions. In this way, a variable separation is introduced and a reduction from a partial differential system (3.2) to a set of ordinary differential equation is allowed. Normal mode solutions of the form

$$\begin{aligned}
\tilde{u}(t,x,y,z) &= \frac{1}{2}\left(\hat{u}+\hat{u}^*\right) = \frac{1}{2}\left[\mathbf{u}(y)\, e^{i(\alpha x+\gamma z-\omega t)} + \mathbf{u}(y)^* e^{i(\alpha^* x+\gamma^* z-\omega^* t)}\right], \\
\tilde{v}(t,x,y,z) &= \frac{1}{2}\left(\hat{v}+\hat{v}^*\right) = \frac{1}{2}\left[\mathbf{v}(y)\, e^{i(\alpha x+\gamma z-\omega t)} + \mathbf{v}(y)^* e^{i(\alpha^* x+\gamma^* z-\omega^* t)}\right], \\
\tilde{w}(t,x,y,z) &= \frac{1}{2}\left(\hat{w}+\hat{w}^*\right) = \frac{1}{2}\left[\mathbf{w}(y)\, e^{i(\alpha x+\gamma z-\omega t)} + \mathbf{w}(y)^* e^{i(\alpha^* x+\gamma^* z-\omega^* t)}\right], \\
\tilde{p}(t,x,y,z) &= \frac{1}{2}\left(\hat{p}+\hat{p}^*\right) = \frac{1}{2}\left[\mathbf{p}(y)\, e^{i(\alpha x+\gamma z-\omega t)} + \mathbf{p}(y)^* e^{i(\alpha^* x+\gamma^* z-\omega^* t)}\right],
\end{aligned} \tag{3.3}$$

are to be found. The quantities $\hat{u}, \hat{v}, \hat{w}, \hat{p}$ indicate the complex normal mode, while $\mathbf{u}(y), \mathbf{v}(y), \mathbf{w}(y), \mathbf{p}(y)$ are functions of the y only and the $*$ quantities are the complex conjugates. Therefore, the sum of the normal mode and its complex conjugate is the real disturbance quantity. The perturbative quantities can be treated separately as the system is linear. In principle, since the complex conjugate values can be obtained from the quantities themselves, it

is only necessary to solve for the complex quantities $\hat{u}, \hat{v}, \hat{w}, \hat{p}$. To be solutions for the perturbations, the modal expansions (3.3) have to satisfy the system (3.2). In this way the partial differential equations system (independent variables t, x, y, z) reduces to a ordinary differential equations system (independent variable y).

Moreover, the amplitude and the phase of the oscillations can be expressed through the use of complex functions, as the eigenvectors $\mathbf{u}(y), \mathbf{v}(y), \mathbf{w}(y), \mathbf{p}(y)$. For any disturbance, in fact, the amplitude of the cosine and the amplitude of the sine components are to be given. This is done through the real and the imaginary parts of the above complex functions, respectively. With a single complex quantity, the two values (phase and amplitude) characterizing the oscillation can be expressed. Substitution of (3.3) into the linearized system (3.2) results in the following set of linear equations

$$\begin{cases} i\alpha\mathbf{u} + \mathbf{v}^{'} + i\gamma\mathbf{w} = 0, \\ \\ i\alpha(U-c)\mathbf{u} + i\alpha\mathbf{p} + U^{'}\mathbf{v} = \dfrac{1}{Re}\left(\mathbf{u}^{''} - (\alpha^2+\gamma^2)\mathbf{u}\right), \\ \\ i\alpha(U-c)\mathbf{v} + \mathbf{p}^{'} = \dfrac{1}{Re}\left(\mathbf{v}^{''} - (\alpha^2+\gamma^2)\mathbf{v}\right), \\ \\ i\alpha(U-c)\mathbf{w} + i\gamma\mathbf{p} = \dfrac{1}{Re}\left(\mathbf{w}^{''} - (\alpha^2+\gamma^2)\mathbf{w}\right). \end{cases} \tag{3.4}$$

In the above relations $\alpha = \alpha_r + i\alpha_i$ and $\gamma = \gamma_r + i\gamma_i$ are identified as complex wavenumbers in x and z direction, rispectively. Real part of these numbers α_r, γ_r are the wavelength of the perturbation in x and z direction, while the imaginary parts α_i, γ_i are the spatial grow rates in the x and z direction, respectively. The complex frequency is $\omega = \omega_r + i\omega_i$, where ω identifies the frequency of the perturbative wave and ω_i is the temporal growth rate. The wave velocity is defined as $c = c_r + ic_i = \omega/\alpha$.

A single equation for $\mathbf{v}$ can now be obtained in a straigthforward manner. The $\mathbf{u}$ momentum equation is multiplied by $i\alpha$ and the $\mathbf{w}$ momentum equation is multiplied by $i\gamma$. The resulting equations are summed and the continuity equation is used to replace the expression $i\alpha\mathbf{u} + i\gamma\mathbf{w}$ with $-\mathbf{v}^{'}$, resulting in the system

$$\begin{cases} i\alpha(U-c)\mathbf{v} + \mathbf{p}^{'} = \dfrac{1}{Re}\left(\mathbf{v}^{''} - (\alpha^2+\gamma^2)\mathbf{v}\right), \\ \\ i\alpha(U-c)\mathbf{v}^{'} + (\alpha^2+\gamma^2)\mathbf{p} - i\alpha U^{'}\mathbf{v} = \dfrac{1}{Re}\left(\mathbf{v}^{'''} - (\alpha^2+\gamma^2)\mathbf{v}^{'}\right). \end{cases} \tag{3.5}$$

The pressure is eliminated by differentiating the second equation of (3.5) by y and then using the first equation (the $\mathbf{v}$ momentum equation), resulting in a single equation for $\mathbf{v}$, namely

$$(U-c)\left(\mathbf{v}'' - (\alpha^2+\gamma^2)\mathbf{v}\right) - U''\mathbf{v} = \frac{1}{i\alpha Re}\left(\mathbf{v}'''' - 2(\alpha^2+\gamma^2)\mathbf{v}'' + (\alpha^2+\gamma^2)^2\mathbf{v}\right). \tag{3.6}$$

The above equation is the three-dimensional Orr-Sommerfeld equation, which is fourth order differential equation. The use of normal mode relationship (3.3) for perturbations substituted into system (3.2) transform the partial differential equations in ordinary differential equations. However, this transformation does not come without complications. Equation (3.6) define a eigenvalue problem, where $\mathbf{v}$ is the eigenfunction and α, γ and ω are the unknowns. So the number of unknowns is increased to six, namely: α_r, α_i, γ_r, γ_i, ω_r, ω_i. In order to overcome this problem, in the next section the Squire transformation is presented.

3.4 Squire transformation

Squire (1933) recognized that, with a simple transformation, equation (3.6) can be reduced to a form equivalent to the two-dimensional Orr-Sommerfeld equations. Define the polar wavenumber $\mathbf{k} = (\alpha, \gamma)$ such that

$$\|\mathbf{k}\| = k = \sqrt{\alpha^2+\gamma^2}, \tag{3.7}$$

and a reduced Reynolds number as

$$Re_{2d} = \frac{\alpha Re}{\sqrt{\alpha^2+\gamma^2}}. \tag{3.8}$$

In such a way, relationship between α, γ and k are

$$\begin{aligned} \alpha &= k\cos\phi, \\ \gamma &= k\sin\phi, \\ \phi &= \tan^{-1}(\gamma/\alpha), \end{aligned} \tag{3.9}$$

where ϕ is the polar angle in wave space, as shown in figure (3.1). Substitution of (3.7) and (3.8) into (3.6) results in:

$$(U-c)\left(\mathbf{v}'' - k^2\mathbf{v}\right) - U''\mathbf{v} = \frac{1}{ikRe_{2d}}\left(\mathbf{v}'''' - 2k^2\mathbf{v}'' + k^4\mathbf{v}\right), \tag{3.10}$$

which has the exact form of two-dimesional Orr-Sommerfeld equation. If the fluid is taken as inviscid ($Re \to \infty$), a second order differential equation

$$(U-c)(\mathbf{v}'' - \alpha^2\mathbf{v}) - U''\mathbf{v} = 0 \tag{3.11}$$

was first derived by Rayleigh (1880) [26] and known as Rayleigh equation. Although often referred as the "inviscid Orr-Sommerfeld" equation, the Rayleigh equation is not a special case ($Re \to \infty$) of the Orr-Sommerfeld equation as it was derived more than 25 years before it.

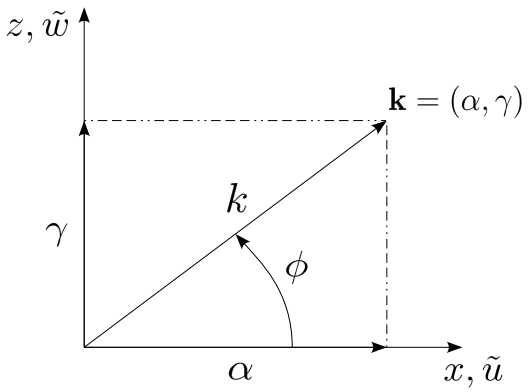

Figure 3.1: A geometric scheme of Squire transformation.

The transformation that takes the three-dimesional problem and transform it into an equivalent two-dimensional problem is called the Squire transformation. For parallel flows, should be studied only the two-dimensional problem for determining stability. Once k and Re_{2d} are determined from the two-dimensional problem, the true wavenumbers α, γ and Re can be determined by inverting the transformation (3.9) for a given polar angle ϕ. The two-dimensional and three-dimensional problems have the same formulation, except that the two-dimensional problem has a lower value of the Reynolds number. Finally, the wave velocity c remains unscaled for the three-dimensional and the two-dimensional problems. All these remarks are summed up in the following theorem

Theorem 3.4.1 (***Squire's Theorem (1933)***). *If an exact two-dimensional parallel flow admits an unstable three-dimensional disturbance for a certain value of the Reynolds number, it also admits a two-dimensional disturbance at a lower value of the Reynolds number.*

In other words the theorem could also be stated as, "*The minimum Reynolds number for instability will be higher for an oblique three-dimensional wave than for a purely two-dimensional one.*" Or, "*To each unstable three-dimensional perturbation there corresponds a two-dimensional one with a lower Reynolds number (and with a higher longitudinal wavenumber).*", in fact, from (3.8)

$$Re_{2d} = \frac{\alpha}{k} Re \;\Rightarrow\; Re_{2d} < Re. \tag{3.12}$$

Therefore, in the framework of the normal mode theory, only two-dimensional perturbations will be considered. Anyhow, it should be reminded that the Squire theorem only applies to parallel flows. For more complicated flows, such as three-dimensional or curved mean flows, three-dimensional perturbations have to be considered. Moreover, theorem (3.4.1) does not exclude the possibility that, for sufficiently high Reynolds number values, an unstable oblique wave can occur even if the corresponding two-dimensional one (with the same longitudinal wavenumber k) is stable.

3.5 Stability criterion in normal mode analysis

In section (2.2) a general definition of stability is given. The definition is related to a measure of the size of the perturbation and so to its amplitude. In the more general spatio-temporal stability analysis, α, γ and ω are complex. By using the normal mode expansion (3.3) the amplitudes of the perturbative functions $\tilde{u}$, $\tilde{v}$, $\tilde{w}$ and $\tilde{p}$ are proportional to $e^{-\alpha_i x - \gamma_i z + \omega_i t}$. In this way the fate of stabilty is given by the sign of coefficient α_i, γ_i and ω_i.

The wave velocity is defined as $c = c_r + ic_i = \omega/\alpha$, while the phase velocity is $v_p = \omega_r/k$. For the temporal evolution, if $\omega_i > 0$ for one mode, the corresponding perturbation exponentially grows until the non-linearities become relevant to the system. The mode is *unstable*. If $\omega_i = 0$ the mode is *marginally stable*, while if $\omega_i < 0$ the mode is *stable*. In general, as a small perturbation can excite all the modes, it is sufficient that $\omega_i > 0$ for only one mode to have an unstable configuration for the flow. On the contrary, it is necessary that $\omega_i < 0$ for all the modes to have a stable configuration.

Similar considerations can be made for the spatial evolution. If $\alpha_i < 0$ and $\gamma_i < 0$ for one mode the flow is *spatially unstable*. On the contrary, if both $\alpha_i, \gamma_i \geq 0$ for all the modes the flow is *spatially stable*. To separately consider the temporal and the spatial stability it is sufficient to let $\alpha_i = 0$, $\gamma_i = 0$ and $\omega_i = 0$, respectively.

Imposing Re and the perturbed base flow, and solving eigenvalue problem (3.10), the asymptotic fate of perturbation can be seen. Figure (3.2) shows the stability region in plane $(Re - k)$. Every point of this plane is characterized by *stability*, *marginal stability* or *instability*. In particular there are three regions and, for a fixed wavenumber k, a *critical Reynolds number* Re_c can be defined as the lowest Reynols number at which every wavenumber is stable. From figure (3.2) can be noticed that, for a fixed wavenumber k, a flow initially stable can become unstable by increasing its velocity.

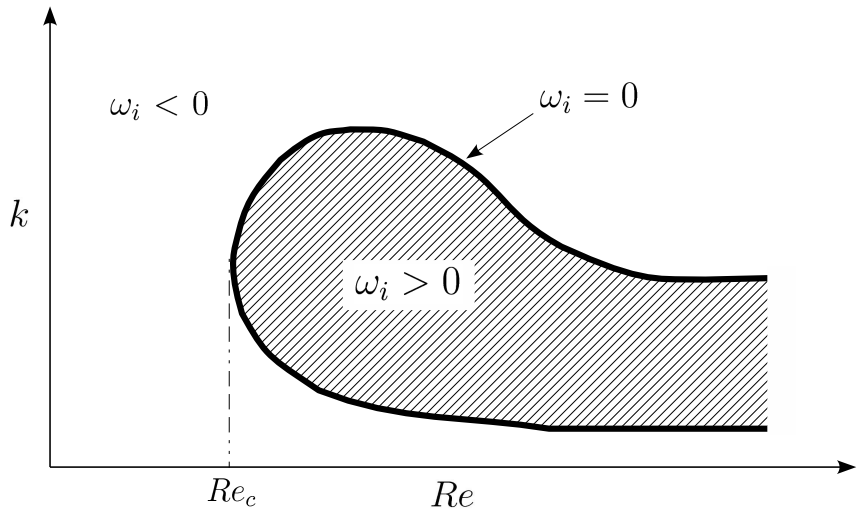

Figure 3.2: General form of stability loop for shear flows.

3.6 Dispersion relation: convective and absolute

The Orr-Sommerfeld eigenvalue problem (3.10) can be expressed as

$$[A(k; Re) + cB(k)]\mathbf{v} = 0 \tag{3.13}$$

where A and B are square and, in general, complex matrices. In principle, a nontrivial solution of the homogeneous system can be obtained by imposing that

$$\det[A(k; Re) + cB(k)] = 0. \tag{3.14}$$

However, the analytical solution of the problem is given only for very simple base flow profiles (e.g. piecewise linear profiles). Numerical means are usually required for more complicate velocity profiles. From the general solution of the Orr-Sommerfeld equation at a fixed Re, the dispersion relation between the wavenumber and the frequency can be obtained

$$\mathcal{D}(k, \omega; Re) = 0. \tag{3.15}$$

and the explicit form holds

$$\omega = \omega(k; Re). \tag{3.16}$$

The dispersion relation gives significant information about the stability characteristics k and ω, as a discrete set of eigenvalues ω_n (with k and Re parameters) can be found. Imposing Re and the perturbed base flow, and solving

eigenvalue problem (3.14), the asymptotic fate of perturbation can be seen. Figure (3.2) shows the stability region in plane $(Re - k)$. Every point of this plane is characterized by *stability*, *marginal stability* or *instability*. In particular there are three regions and a *critical Reynolds number* Re_c can be defined as the lowest Reynolds number at which every wavenumber is stable. From figure (3.2) can be noticed that, for a fixed wavenumber k, a flow initially stable can become unstable by increasing its Reynolds number, i.e. its velocity. Moreover, expression (3.16) is fundamental for a deeper stability analysis involving the velocity group definition and the saddle point perturbative hypothesis. First, the complex group velocity $v_g = \partial\omega/\partial k$ is defined as the velocity of a wave packet evolving in time and space. Second, a saddle point of the dispersion relation occurs when the velocity group v_g vanishes, that is

$$\frac{\partial \omega}{\partial k} = 0. \tag{3.17}$$

In these regions of the phase space, the perturbation can grow in time as there is a local increase of energy. In this context, the instability is defined as convective if $\omega_i < 0$ for all the modes and if, for at least one mode, $\alpha_i < 0$ and $\gamma_i < 0$ with group velocity v_g equal to zero. If the coordinate system is moving with the phase velocity of the wave the perturbation is amplified, but it remains small at a fixed point as time passes. The disturbance is convected away. The instability is *absolute* if, for at least one mode, $\omega_i > 0$ and the group velocity v_g vanishes. The perturbation is locally growing in time. The linear theory allows to describe the onset of instability as, when a perturbation establishes, its first behaviour is exponential. However, the subsequent temporal evolution is modified by the non-linear dynamics. This interaction makes the perturbations assume a behaviour which is no longer exponential. Therefore, the linearized equations are useful to study the onset and a possible development of the instability, and not to consider its following evolution.

Chapter 4

IVP: Temporal behaviour of small perturbations

4.1 Introduction

The three-dimensional wake stability has been widely studied by means of normal mode analysis (see section 3.3). However, as previously stated, in this way only the asymptotic fate can be determined, regardless the transient behaviour and the underlying physical cause of any instability. Recent shear flows studies ([7], [10], Criminale et al. 1991 [11]) have been showing the importance of the early time dynamics, which can in principle lead to non-linear growth long before an exponential mode occurs. The recognition of the existence of an algebraic growth, due (among other things) to the non-orthogonality of the eigenfunctions (Sommerfeld 1949 [31]) and a possible resonance between Orr-Sommerfeld and Squire solutions [2], recently promoted many contributions directed to study the early-period dynamics. For fully bounded flows works by Criminale et al. 1991 [11], Criminale et al. 1997 [13], [17], [3], [27], [28], and for partially bounded flows works by Lasseigne et al. 1999 [22], [19], [14], can be cited. As for free shear flows, the attention was first aimed to obtain closed-form solutions to the initial-value inviscid problem ([6]; Criminale et al. 1995 [12]) by considering piecewise linear parallel basic flow profiles. Recently, by means of multiscale approach, explicit solutions have been obtained for continuous parallel base flow profiles ([8]). The initial-value problem is here extended to include, in the stability analysis, a more accurate description of the mean flow. In particular, the longitudinal component of the Navier-Stokes expansion solutions is considered, so that the problem is parameterized on x_0 (the longitudinal coordinate) and the Reynolds number Re. The formulation will be carried on similarly to

what first proposed by Criminale & Drazin (1990) [10]. Early transient and asymptotic behaviour are examined for the base flow configurations corresponding to Reynolds numbers ($Re = 50; 100$) of the order of the critical value for the onset of the first instability, and for longitudinal sections x_0 inside the intermediate region of the flow where the entrainment process is working. Different physical inputs (linked to the shape, the obliquity, the length and the symmetry of the perturbation) which most influence the subsequent temporal evolution are presented. In the initial-value problem formulation, the introduction of a complex wavenumber in the streamwise direction is an innovative feature suggested by the combined spatio-temporal modal stability analysis. The imaginary part of the complex longitudinal wavenumber, which determines the longitudinal evolution of the perturbing wave, plays an important role in the whole temporal evolution of the perturbation. In fact, varying the order of magnitude of this parameter leads to actually different temporal trends. A longitudinal asymptotic comparison with modal results (carried out considering arbitrary initial conditions and not waves related to the most unstable mode) is made. It can be demonstrated that the agreement is good for both the frequency as well as the temporal growth rate.

4.2 The initial-value problem

4.2.1 Formulation

The first orders ($n = 0; 1; 2$) of the inner longitudinal component velocity field are taken as a first approximation of the base flow, [1]. The analytical expression is reported below for convenience

$$U(y; x_0, Re) = 1 - \frac{a\, C_1}{\sqrt{x_0}}\, e^{-\frac{Re}{4}\frac{y^2}{x_0}}, \tag{4.1}$$

where a is related to the drag coefficient, ($a = 1/4(Re/\pi)^{1/2} C_D(Re)$) and $C_1 = 1.22 + 0.000067\, Re^2$; is a integration constant that depends on the Reynolds number. By changing the longitudinal coordinate x_0, which plays the role of parameter together with the Reynolds number, the base flow profile (7.1) will locally approximate the behaviour of the actual wake generated by the body. The wake sections taken into account are in the interval $3 \leq x_0 \leq 50$. Base flow configurations corresponding to a Re of $50; 100$ are considered. In figure (4.1) a representation of the wake profile at differing longitudinal stations is shown. The continuity and Navier-Stokes equations

(describing the system perturbed with small disturbances) are linearized and expressed as

$$\begin{cases} \dfrac{\partial \tilde{u}}{\partial x} + \dfrac{\partial \tilde{v}}{\partial y} + \dfrac{\partial \tilde{w}}{\partial z} = 0, \\ \dfrac{\partial \tilde{u}}{\partial t} + U\dfrac{\partial \tilde{u}}{\partial x} + \tilde{v}U' + \dfrac{\partial \tilde{p}}{\partial x} = \dfrac{1}{Re}\nabla^2\tilde{u}, \\ \dfrac{\partial \tilde{v}}{\partial t} + U\dfrac{\partial \tilde{v}}{\partial x} + \dfrac{\partial \tilde{p}}{\partial y} = \dfrac{1}{Re}\nabla^2\tilde{v}, \\ \dfrac{\partial \tilde{w}}{\partial t} + U\dfrac{\partial \tilde{w}}{\partial x} + \dfrac{\partial \tilde{p}}{\partial z} = \dfrac{1}{Re}\nabla^2\tilde{w}. \end{cases} \tag{4.2}$$

where $\tilde{u}(t,x,y,z), \tilde{v}(t,x,y,z), \tilde{w}(t,x,y,z)$ and $\tilde{p}(t,x,y,z)$ are the perturbation velocity and pressure respectively. The independent spatial variables z and y are defined from $-\infty$ to $+\infty$, x from 0 to $+\infty$. All physical quantities are normalized with respect to the free stream velocity, the spatial scale of the flow D and the density. By combining motion equations of (4.2) to eliminate the pressure terms, the *curl* operator is applyed

$$\begin{cases} \dfrac{\partial \tilde{\omega}_x}{\partial t} + U\dfrac{\partial \tilde{\omega}_x}{\partial x} - \dfrac{1}{Re}\nabla^2\tilde{\omega}_x = -U'\dfrac{\partial \tilde{w}}{\partial x}, \\ \dfrac{\partial \tilde{\omega}_y}{\partial t} + U\dfrac{\partial \tilde{\omega}_y}{\partial x} - \dfrac{1}{Re}\nabla^2\tilde{\omega}_y = -U'\dfrac{\partial \tilde{v}}{\partial z}, \\ \dfrac{\partial \tilde{\omega}_z}{\partial t} + U\dfrac{\partial \tilde{\omega}_z}{\partial x} - \dfrac{1}{Re}\nabla^2\tilde{\omega}_z = -U'\dfrac{\partial \tilde{w}}{\partial z} + U''\tilde{v}. \end{cases} \tag{4.3}$$

From kinematics is known the relation

$$\tilde{\Gamma} = \nabla^2\tilde{v} = \frac{\partial \tilde{\omega}_z}{\partial x} - \frac{\partial \tilde{\omega}_x}{\partial z}. \tag{4.4}$$

Combining in this way the first and the third equation of (4.3)

$$\begin{cases} \nabla^2\tilde{v} = \tilde{\Gamma}, \\ \dfrac{\partial \tilde{\omega}_y}{\partial t} + U\dfrac{\partial \tilde{\omega}_y}{\partial x} - \dfrac{1}{Re}\nabla^2\tilde{\omega}_y = -U'\dfrac{\partial \tilde{v}}{\partial z}, \\ \dfrac{\partial \tilde{\Gamma}}{\partial t} + U\dfrac{\partial \tilde{\Gamma}}{\partial x} - \dfrac{1}{Re}\nabla^2\tilde{\Gamma} = U''\dfrac{\partial \tilde{v}}{\partial x}. \end{cases} \tag{4.5}$$

In so doing, the three coupled equations (4.5) describe the perturbed system. The second and the first equation are the Squire and Orr-Sommerfeld equations respectively, known from the classical linear stability analysis for three-dimensional disturbances and written in partial differential equation form. From kinematics, the relation (4.4) physically links together the perturbation vorticity in the x and z directions ($\tilde{\omega}_x$ and $\tilde{\omega}_z$, respectively) and the perturbation velocity field.

The three equations of (4.5) fully describes the perturbed system in terms of vorticity. This formulation is not that common in linear stability analysis, although the dynamics description is physically more appropriate in terms of vorticity than velocity. For continuous profiles, the governing perturbative equations cannot be analytically solved in general, but they assume a reduced form in the free stream (Blossey et al. 2007 [8]). Equations of (4.5) show that the only cause of any perturbation vorticity production is the interaction between the mean vorticity in z-direction ($\Omega_z = -dU/dy$) and the perturbation strain rates in x and z directions ($\partial\tilde{v}/\partial x$ and $\partial\tilde{v}/\partial z$, respectively).

4.2.2 Laplace-Fourier transforms

The perturbations are Laplace and Fourier decomposed in the x and z directions, respectively. A complex wavenumber $\alpha = \alpha_r + i\alpha_i$ along the x coordinate, as well as, a real wavenumber γ along the z coordinate are introduced. In order to have a finite perturbation kinetic energy, the imaginary part α_i of the complex longitudinal wavenumber can only assume non-negative values. In so doing, perturbative waves can spatially decay ($\alpha_i > 0$) or remain constant in amplitude ($\alpha_i = 0$). The perturbation quantities ($\tilde{v}, \tilde{\Gamma}, \tilde{\omega}_y$) involved in the system dynamics are now indicated as ($\hat{v}, \hat{\Gamma}, \hat{\omega}_y$), where

$$\hat{f}(y,t;\alpha,\gamma) = \int_{-\infty}^{+\infty}\int_{0}^{+\infty} \tilde{f}(x,y,z,t)\, e^{-i(\alpha x+\gamma z)}\, dx\, dz \tag{4.6}$$

indicates the Laplace-Fourier transform of a general dependent variable in the $\alpha - \gamma$ phase space and in the remaining independent variables y and t. The transformed governing partial differential equations are

$$
\begin{cases}
\dfrac{\partial^2 \hat{v}}{\partial y^2} - \left(k^2 - \alpha_i^2 + 2ik\cos\phi\alpha_i\right)\hat{v} = \hat{\Gamma}, \\
\dfrac{\partial \hat{\omega}_y}{\partial t} = -\left(ik\cos\phi - \alpha_i\right) U\hat{\omega}_y - ik\sin\phi\dfrac{dU}{dy}\hat{v} + \\
\qquad + \dfrac{1}{Re}\left[\dfrac{\partial^2 \hat{\omega}_y}{\partial y^2} - \left(k^2 - \alpha_i^2 + 2ik\cos\phi\alpha_i\right)\hat{\omega}_y\right], \\
\dfrac{\partial \hat{\Gamma}}{\partial t} = \left(ik\cos\phi - \alpha_i\right)\left(\dfrac{d^2U}{dy^2}\hat{v} - U\hat{\Gamma}\right) + \\
\qquad + \dfrac{1}{Re}\left[\dfrac{\partial^2 \hat{\Gamma}}{\partial y^2} - \left(k^2 - \alpha_i^2 + 2ik\cos\phi\alpha_i\right)\hat{\Gamma}\right].
\end{cases}
\tag{4.7}
$$

where $\phi = \tan^{-1}(\gamma/\alpha_r)$ is the perturbation angle of obliquity with respect to the $x-y$ physical plane, $k = \sqrt{\gamma^2 + \alpha_r^2}$ is the polar wavenumber and $\alpha_r = k\cos\phi$, $\gamma = k\sin\phi$ are the wavenumbers in x and z directions respectively. The imaginary part α_i of the complex longitudinal wavenumber is a spatial damping rate in streamwise direction. In figure (4.1) the three-dimensional perturbative geometry scheme is shown. In particular the effect of obliquity angle on perturbation is shown in figures (4.2), (4.3) and (4.4). From equations (4.7), it can be noted that there can't be either advection or production of vorticity in the free stream. Vorticity can only be diffused as just the diffusive terms remain when $y \to \infty$. Perturbation vorticity vanishes in the free stream, regardless if it is initially inserted there (if inserted, vorticity is finally dissipated in time when $y \to \infty$). This means that the velocity field is harmonic if $y \to \infty$.

The introduction, through the Laplace decomposition in x-direction, of a complex wavenumber α is an innovative feature, as it permits to carry out a combined spatiotemporal linear stability analysis that is a quite standard procedure for normal mode theory, but is not that common for initial-value problems. Both transient behaviour and asymptotic fate of the disturbances will be discussed in the following considering the resulting influence of this new characteristic. Combining Fourier transformed continuity equation

$$
-\frac{d\hat{v}}{dy} = i\alpha\hat{u} + i\gamma\hat{w},
$$

with Fourier transformed definition of vorticity along y

$$
\hat{\omega}_y = i\gamma\hat{u} - i\alpha\hat{w},
$$

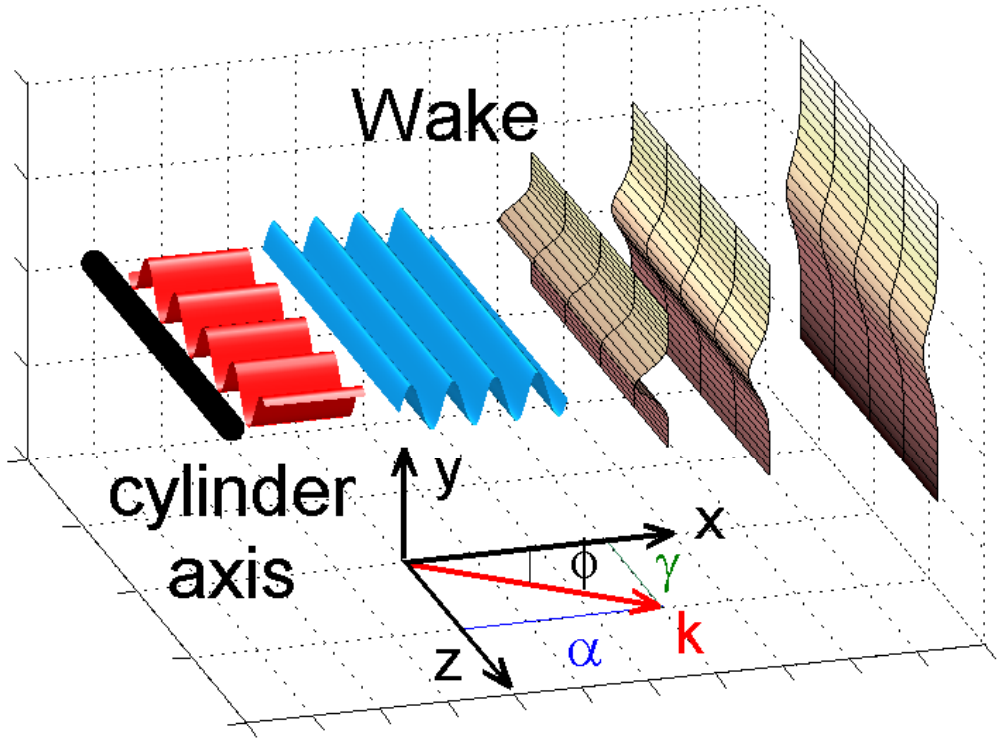

Figure 4.1: Perturbation scheme. Red and blue waves represents perturbations with obliquity angle $\phi = 0$, and $\pi/2$ respectively. Gray surfaces represents the base flow profile $U(y; x_0, Re)$ at distances $x_0 = 5D$, $10D$, $15D$ from the cylinder where D is the cylinder diameter

gives

$$\begin{aligned} \hat{u} &= \frac{i}{k^2}\left(-\gamma\,\hat{\omega}_y + \alpha\,\frac{d\hat{v}}{dy}\right), \\ \hat{w} &= -\frac{i}{k^2}\left(\alpha\,\hat{\omega}_y + \gamma\,\frac{d\hat{v}}{dy}\right). \end{aligned} \tag{4.8}$$

Once system (4.7) is solved and $\hat{v}$, $\hat{\omega}_y$ are known, one can use the above relations (4.8) to find $\hat{u}$ and $\hat{w}$.

4.2.3 Initial and boundary conditions

Governing equations (4.7) need proper initial and boundary conditions to be solved. Among all solutions, those whose perturbation velocity field is zero in the free stream are sought. Periodic initial conditions for

$$\frac{\partial^2 \hat{v}}{\partial y^2} - \left(k^2 - \alpha_i^2 + 2ik\cos\phi\alpha_i\right)\hat{v} = \hat{\Gamma}, \tag{4.9}$$

can be shaped in terms of set of functions in the L2 Hilbert space, as

$$\hat{v}(0,y) = e^{-(y-y_0)^2}\cos\left(n_0(y-y_0)\right), \quad \hat{v}(0,y) = e^{-(y-y_0)^2}\sin\left(n_0(y-y_0)\right),$$

for the symmetric and the asymmetric perturbations, respectively. Parameter n_0 is an oscillatory parameter for the shape function, while y_0 is a parameter which controls the distribution of the perturbation along y (by moving away or bringing nearer the perturbation maxima from the axis of the wake). The transversal vorticity $\hat{\omega}_y(0,y)$ is chosen initially equal to zero throughout the y domain, to directly observe which is the net contribution of three-dimensionality on the transversal vorticity temporal evolution. Results will later show how the initial introduction of normal vorticity can influence the evolution of disturbances. The trigonometrical system is a Schauder basis in each space $L^p[0;1]$, for $1 < p < 1$. More specifically, the system $(1, \sin(n_0,y), \cos(n_0,y), \dots)$, where $n_0 = 1, 2, \dots$, is a Schauder basis for the space of square-integrable periodic functions with period 2π. This means that any element of the space L^2, where the dependent variables are defined, can be written as an infinite linear combination of the elements of the basis. Once initial and boundary conditions are properly set, the partial differential equations (4.7) are numerically solved by method of lines on a spatial finite domain $[-y_f, +y_f]$. The value y_f is chosen so that the numerical solutions are insensitive to further extensions of the computational domain size. Here, y_f is of the order of magnitude 10^1, i.e. $y_f \approx 3\lambda$ where λ is the perturbation's wavelength ($\lambda = 2\pi/k$). The spatial derivatives are centre differenced and the resulting system is then integrated in time by an adaptative multi-step method (variable order Runge-Kutta (2,3) pair of Bogacki & Shampine ODE solver).

4.3 Measure of the growth

One of the salient aspects of the IVP is the early transient evolution of various initial conditions. To this end, a measure of the perturbation growth can be defined through the disturbance kinetic energy density in the plane (α, γ)

$$e(t,\alpha,\gamma,Re) = \frac{1}{2}\frac{1}{2y_d}\int_{-y_d}^{y_d}\left(|\hat{u}|^2 + |\hat{v}|^2 + |\hat{w}|^2\right)dy, \tag{4.10}$$

that could be also expressed as

$$e(t,\alpha,\gamma,Re) = \frac{1}{2}\frac{1}{2y_d}\frac{1}{|\alpha^2+\gamma^2|}\int_{-y_d}^{y_d}\left(\left|\frac{\partial\hat{v}}{\partial y}\right|^2 + \left|\alpha^2+\gamma^2\right|\left|\hat{\omega_y}\right|^2 + |\hat{w}|^2\right)dy,$$

where $2y_d$ is the extension of the spatial numerical domain. The value y_d is defined so that the numerical solutions are intensitive to further extensions of the computational domain size. The length y_d is taken in function of the wavenumber k, in particular

$$y_d = 40, \quad k \in [\,0.45\,,0.7\,],$$

$$y_d = 30, \quad k \in [\,0.75\,,1\,],$$

$$y_d = 20, \quad k \in [\,1.2\,,500\,].$$

The total kinetic energy can be obtained by integrating the energy density over all α_r and γ. The amplification factor $G(t)$ can be introduced in terms of the normalized energy density

$$G(t,\alpha,\gamma) = \frac{e(t;\alpha,\gamma)}{e(t=0;\alpha,\gamma)}. \tag{4.11}$$

This quantity can effectively measure the growth of a disturbance of wavenumbers (α,γ) at the time t, for a given initial condition at $t=0$ (Criminale et al. 1997 [13]; Lasseigne et al. 1999 [22]). Computations to evaluate the long-time asymptotics are made integrating the equations forward in time beyond the transient, until become true the condition $|dG/dt| < 10^{-4}$ for stable wavenumbers, and $|dG/dt| > 10^4$, for unstable wavenumbers.

The angular frequency (pulsation) ω of the perurbation can be introduced by defining a local, in space and time, time phase φ of the complex wave at a fixed transversal station (for example $y=1$) as

$$\hat{v}(y,t;\alpha,\gamma,Re) = A_t(y;\alpha,\gamma,Re)\,e^{\,i\varphi(t)}, \tag{4.12}$$

and then computing the time derivative of the phase perturbation φ

$$\omega(t) = \frac{d\varphi(t)}{dt}. \tag{4.13}$$

Because φ is defined as the phase variation in time of the perturbative wave, it is reasonable to expect constant values of frequency, once the asymptotic state is reached.

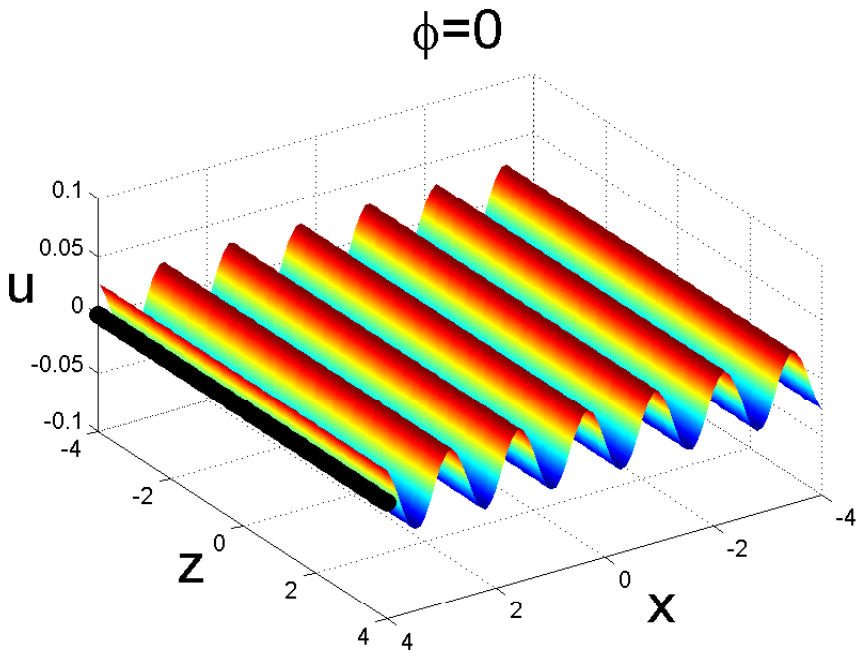

Figure 4.2: Perturbation wave with obliquity angle $\phi = 0$

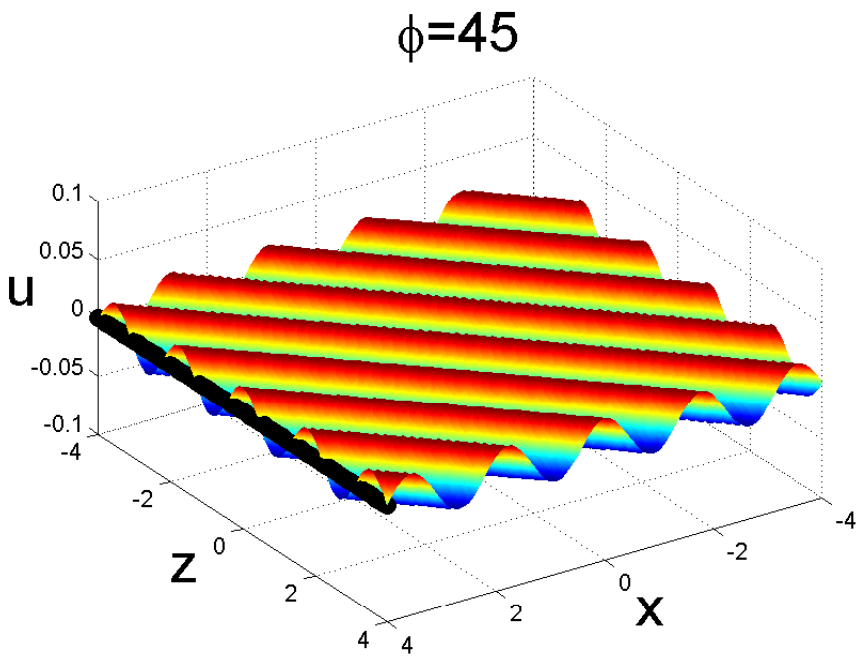

Figure 4.3: Perturbation wave with obliquity angle $\phi = \pi/4$

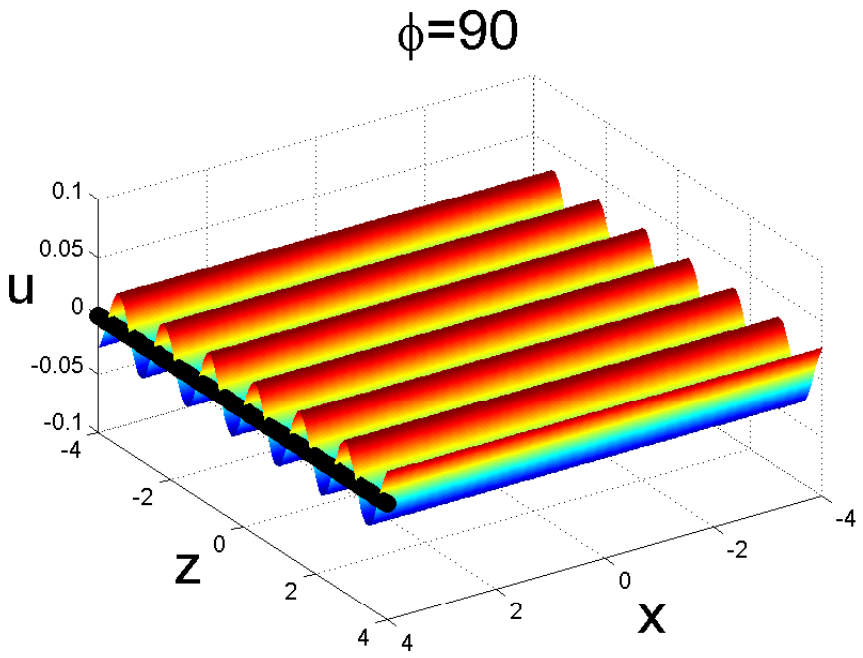

Figure 4.4: Perturbation wave with obliquity angle $\phi = \pi/2$

Chapter 5

Exploratory analysis of the transient dynamics

The linear stability of the two-dimensional wake is studied as a three-dimensional initial-value problem through the formulation presented in the previous chapter. Two main innovative features are introduced here. First, the mean flow (which is parameterized with respect to the Reynolds number and the longitudinal coordinate) is approximated through the longitudinal component of the inner Navier-Stokes expansion 4.1 (see [1]) to include the slow spatial evolution of the system in the stability analysis. Then, a complex wavenumber in streamwise direction is considered when the transformation to the phase space is performed. The leading equations are no more explicitly solvable, but numerical means are required. In synthesis, Laplace and Fourier decompositions are performed in streamwise and spanwise directions, respectively. The perturbation is characterized by real streamwise and spanwise wavenumbers, and a uniform or damped spatial distribution along the longitudinal direction. Amplified streamwise distributions are not considered since the perturbation kinetic energy is required to be finite. The resulting equations in the phase space are numerically solved after appropriate initial and boundary conditions are imposed. In 5.1, an exploration of different transient configurations will be shown with particular attention to those parameters (such as the angle of obliquity, the length and the symmetry of the initial condition) which most affect the early growth and the asymptotic fate. In section 5.2 the perturbation asymptotic states are reproduced and, in the longitudinal case, it can be demonstrated that the agreement with modal analysis turns out to be good for both symmetric and asymmetric initial conditions. Concluding remarks are discussed in 5.4.

5.1 Transient evolution: parameter sensitivity analysis

There are five parameters which play an important role in this perturbative system evolution, these are the Reynolds number (Re), the wake configuration (x_0), the symmetric/asymmetric initial condition properties and the obliquity angles (ϕ), and the wavenumbers k. Since the problem has a lot of parameters, the analysis below is made changing one or two of them at the same time.

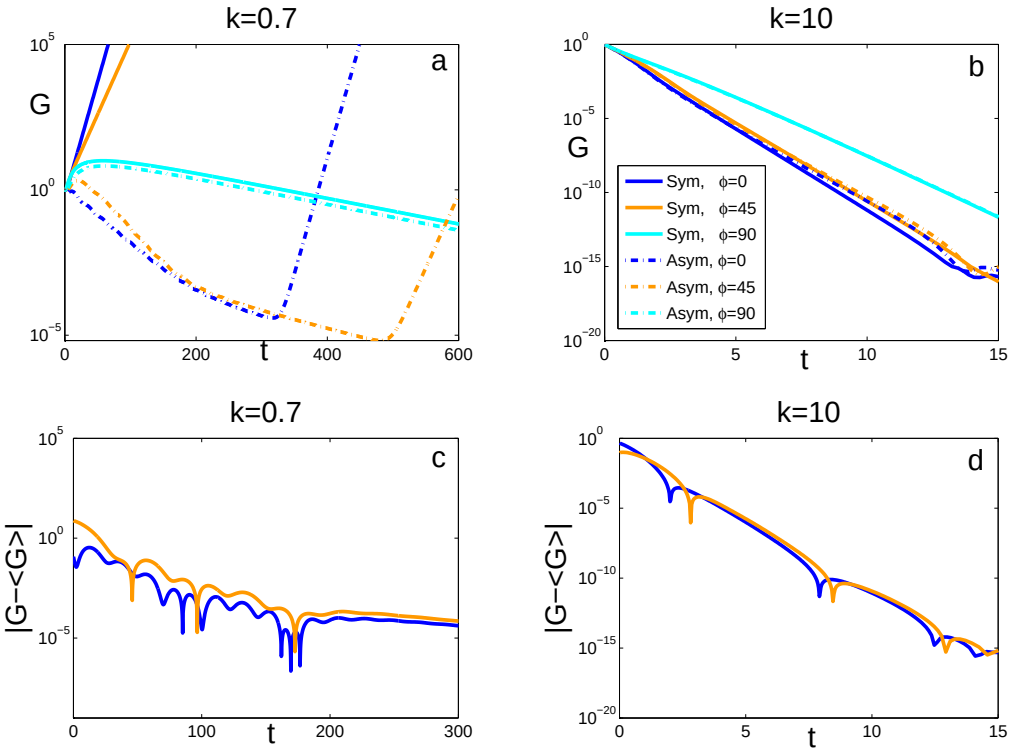

Figure 5.1: The growth factor G, obtained at high Reynolds number ($Re = 100$), intermediate field configuration ($x_0 = 10$), with all possible combinations among asymmetric or symmetric initial condition and obliquity angle ($\phi = 0,\ \pi/4,\ \pi/2$). On the left is shown a case of small wavenumber ($k = 1$) and on the right a case of large wavenumber ($k = 10$).

It is evident that long waves (i.e. waves with a small wavenumber) can become unstable with determinated values of obliquity angles. From the left picture of figure (5.1) can be deduced that exist a value of obliquity angle between $\pi/4$ and $\pi/2$ that distinguishes the two kind of beaviour (stable

or unstable). Moreover the unstable perturbation with asymmetric initial condition have a much longer transient (like 100 times bigger).

The figure on the right shows a beaviour that is more universal, i.e. the effect of the initial condition is realatively small. It can be only observed that all the perturbations are stable. Both graphics show that the longitudinal perturbations ($\phi = 0$) have the fastest evolution, while the pure transversal ones ($\phi = \pi/2$) have the slowest transient.

This particular case shows a behaviour that is generally observed in this analisys, that is, *asymmetric conditions lead to transient evolutions that is last longer than the corrisponding symmetric ones*, and demonstrates that *the transient growth for a longitudinal wave is faster than transversal ones.*

Another feature could be noticed whatching the first part of the transient. As shown in figure (5.1) and (5.1) the transient shows a modulation. The modulation corresponds to a modulation in amplitude of the pulsation of the instability wave (see [10]). The quantity $\left|G - \bar{G}\right|$, (where $\bar{G}$ is the line that have the best fit with G in the mean square root error sense) measure the obscillation of G between $\bar{G}$. Should be noted that this modulation occurs in every solution, but in some is more evident.

The appearence of different scales associated to the different perturbation wavelengths suggests that a self-similarity approach should be adopted to describe the temporal evolution. A continuous instantaneous normalization can be used by defining

$$t^* = t/\tau,$$

with

$$\tau = \frac{G(t)}{\left|\frac{dG}{dt}\right|}.$$

It should be noted that a subset of intermediate-short range waves showing self-similarity features can be observed. It should be noted that a sub set of intermediate-short waves ($k \in [6, 100]$) showing self-similarity features can be observed. Assuming that for this range the amplification factor distribution is scale invariant, then

$$G(\lambda t) = \lambda^h G(t),$$

with unique h. It can be observed, that

$$G(t^*) = G\left(\frac{t}{G(t)/\left|\frac{dG}{dt}\right|}\right) \approx \frac{G(t)}{\tau} = \left|\frac{dG}{dt}\right|,$$

so that $\lambda = 1/\tau$ and $h = 1$. In figure (5.2) the growth factor G is reported as a function of t^*. It should be noted that a subset of long-intermediate waves

showing self-similarity, i.e. for every wavenumber in this subset the energy profiles collapse in only one.

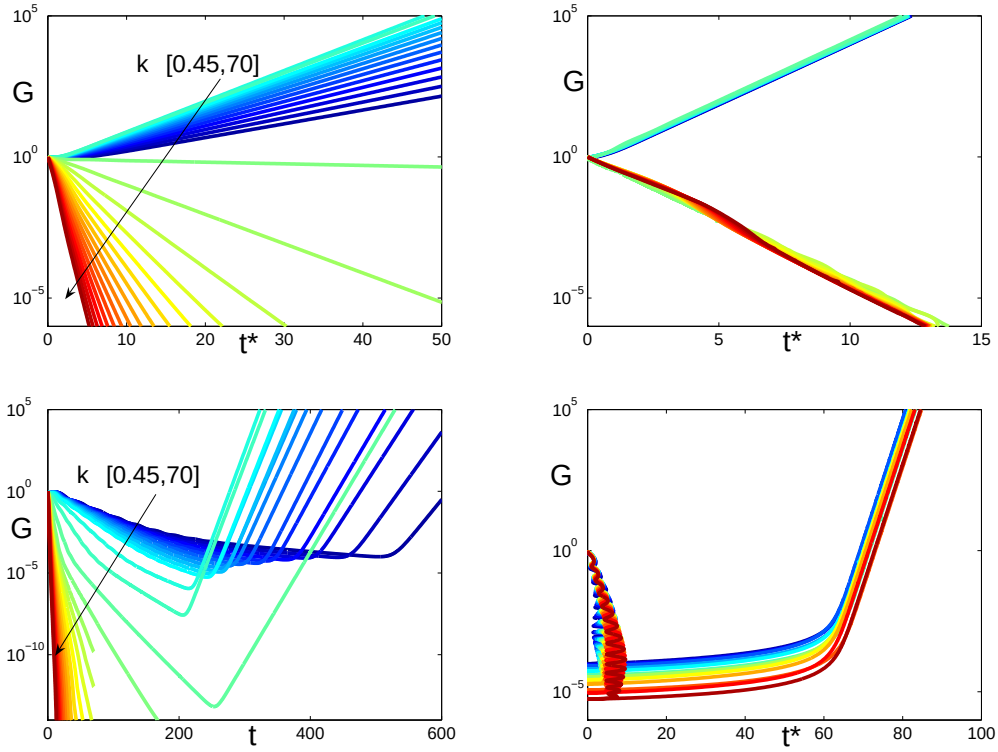

Figure 5.2: Self-similarity.

It is interesting to analyze the combined effect of Reynolds number and wake configuration. In figure (5.3) is showed a comparision between amplification growth factors $G(t)$ of perturbations with a small and large wavenumber.

It shows the G evolution in the system that evolve at different Reynolds number and both the wake configurations. It is evident that

- the far wake configuration have a slower transient with each Reynolds numbers than the intermediate one,
- fixed x_0 the transient evolution goes faster as the Reynolds number increase,
- as the Reynolds number increase the unstable range become bigger too.

This sensitivity analysis can be concluded observing that fixed Reynolds numbers, wake configuration, and obliquity angle the slowest amplification

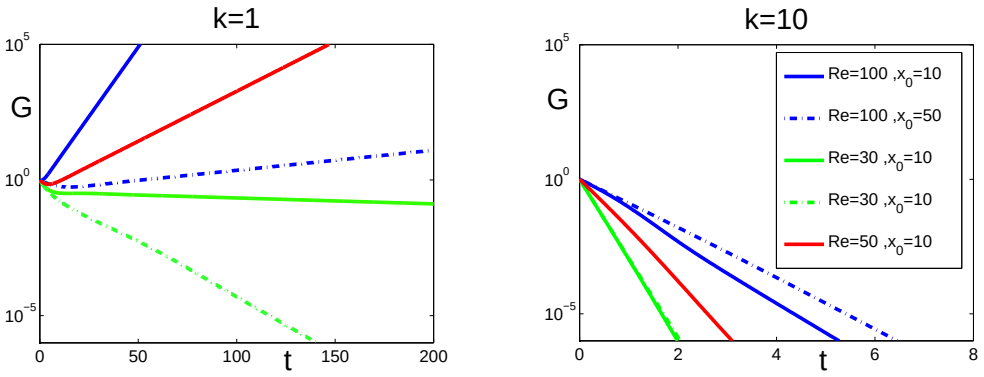

Figure 5.3: The growth factor G, obtained by all possible combination among high Reynolds number ($Re = 100, 50, 30$) and itermediate field wake configuration $x_0 = 10, 50$, for longitudinal waves ($\phi = 0$) and symmetric initial condition. In the left picture is shown an example of small wavenumber ($k = 1$) while in the right a case of large wavenumber ($k = 10$).

factor G evolutions are always related to the link stable and unstable behaviours.

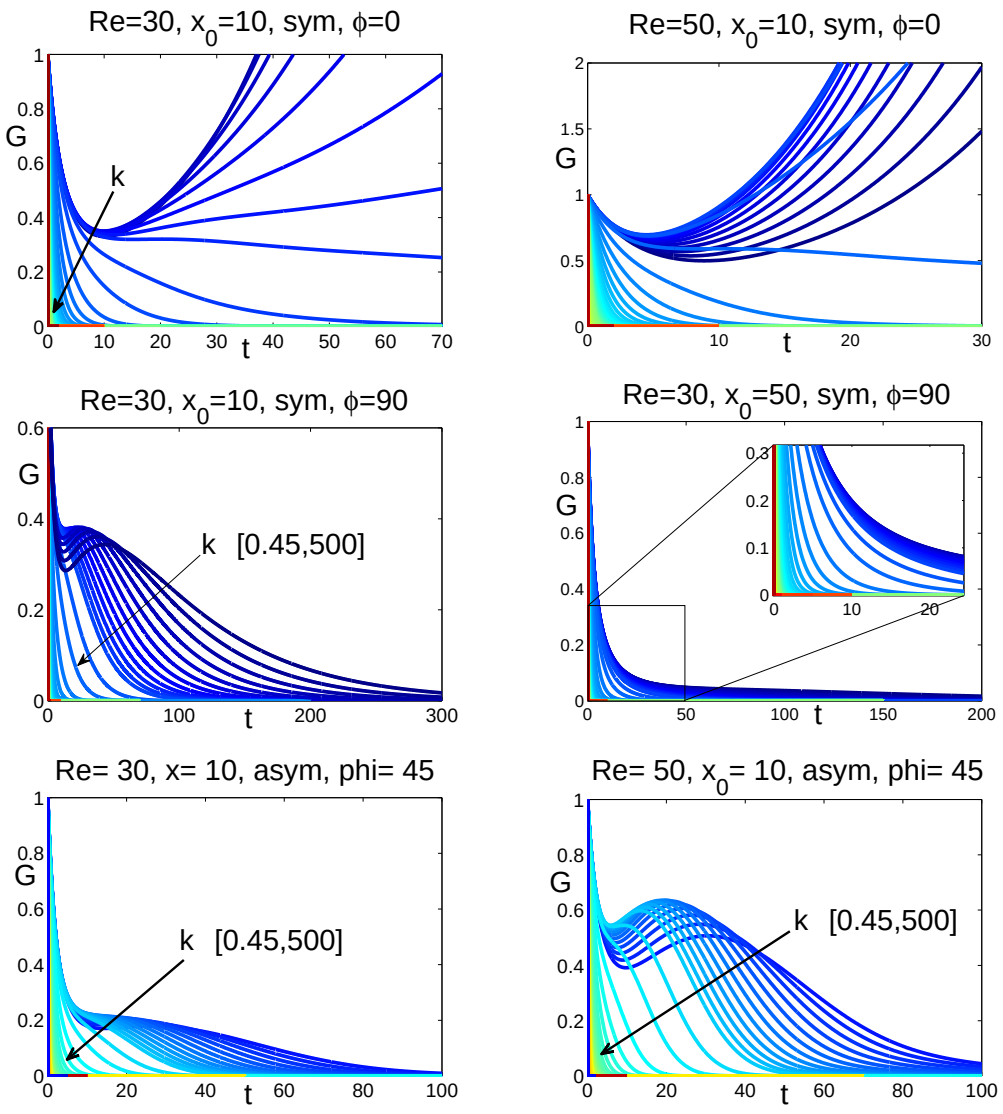

Figure 5.4: Energy transient.

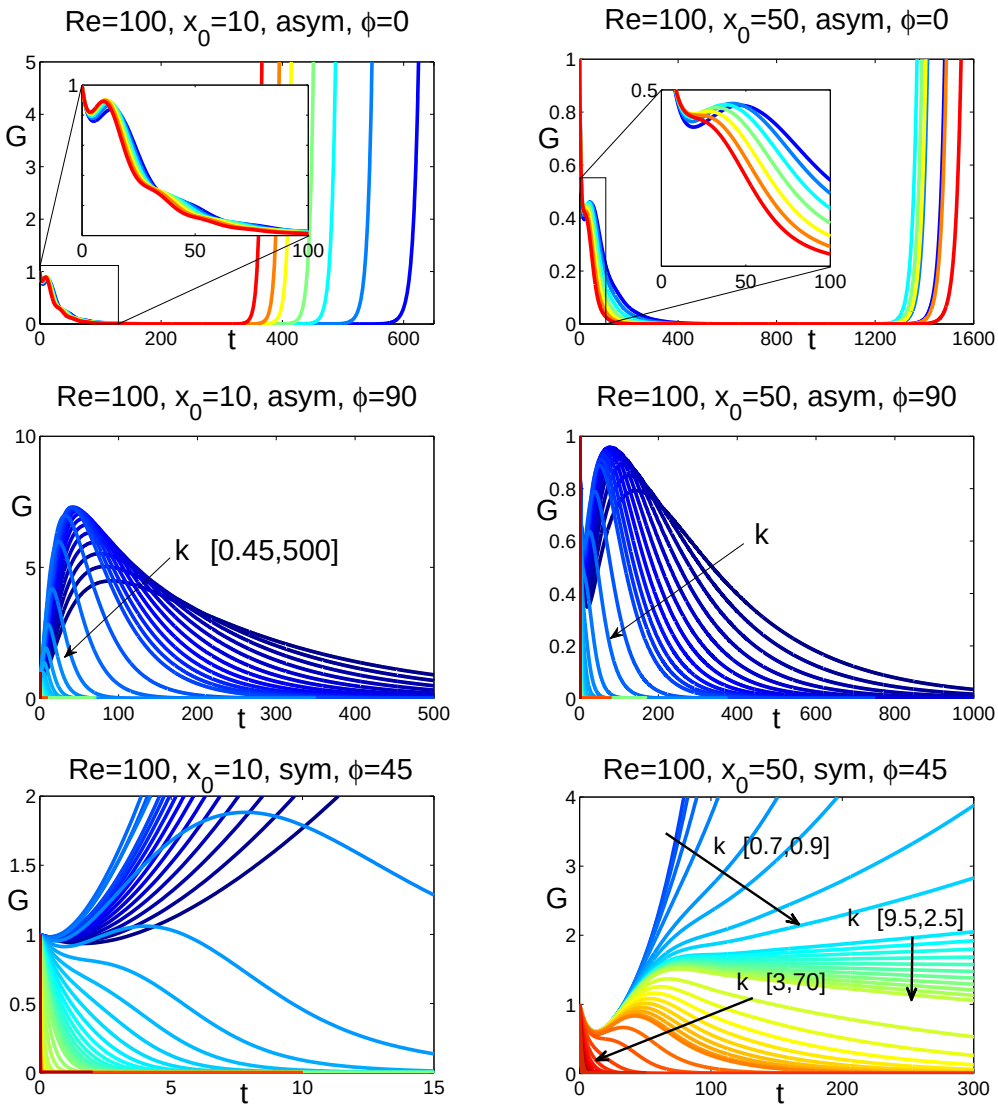

Figure 5.5: Energy transient.

5.2 Perturbation energy spectra

The aim of the thesis is to investigate and quantify the role of nonlinear interaction between different modes of turbulent flow. The focus will be put on the very different scenarios that may occur in the transient for arbitrary small three-dimensional perturbations imposed on a free shear flow. In particular one wants to understand what extent spectral representation highlights the non linear interaction among different scale in comparision to the perturbative state.

It is known that instability flows often evolve into an important state of motion called turbulence, with a chaotic three-dimensional vorticity field with a broad spectrum of small temporal and spatial scales. One of the most important results on turbulent field is given by Kolmogorov. Among all his results, the most useful in this study is the $-5/3$ power-law of the energy spectrum over the inertial range in a fully developed turbulence (see section (2.3)).

Since turbulence occurs in asymptotic state one have to define the end of the transient, i.e. the asymptotic state. Now, it is possible to compute even the exponent of the energy spectrum of the inertial range in the perturbative state and compare it with the exponent corrisponding developed turbulent state.

In the case of small perturbation, the nonlinear term is negligible compared to the other terms in the Navier-Stokes. Therefore a linear equation of motion can be used (linear theory of hydrodynamic stability). This equation should be subject to linearized convective transport, molecular diffusion and linearized vortical stretching. Leaving aside nonlinear interaction among the different scales, these features are tantamount to the features of the turbulent state.

Building a temporal observation window for the transient evolution of a large number ($\approx 10^3$) of arbitrary small three-dimensional perturbation acting on a typical shear flow, the resultant flows are subject to all the processes included in the perturbative Navier-Stokes equations.

Two possible situations can appear

- the exponent difference is large and is a quantitative measure of the non linear interaction in spectral terms,
- the exponent difference is small. This would be even more interesting, because it would indicate a much higher level of the universality of the inertial range, which is not necessary, associated to the non linear interaction.

In this section the exponent of the energy spectrum of arbitrary longitudinal and transversal perturbation acting on the bluff-body wake is determined. In order to do this, is important to find the time of ending transient T_e, i.e. the time that perturbation take to get in their asymptotic conditions. The criteria used to determine asymptotic state is

1. $|dG/dt| < \epsilon_{st} = 10^{-4}$, for stable wavenumbers,
2. $|dG/dt| > \epsilon_{un} = 10^{4}$, for unstable wavenumbers.

For stable perturbations, since $G(t)$ is decaying to zero, the time T_e is defined as the first time such that condition 1 is satisfied. Also, since the waves are all in a state of self-similarity, for unstable wavenumbers condition 2 has been introduced. However this criterion is not sufficient, it can be applied only if is known a priori the behaviour of the perturbation.

The energy spectrum is then evaluated when the temporal variation of $G(t)$ of each wave is crossing a threshold. By recalling that $G(t^*) \approx |dG/dt|$ in the intermediate range, the perturbation system can be considered in its asymptotic state. Every wavelength shows a characteristic temporal scale, $\tau_\epsilon(k)$, for which $|dG/dt|$ satisfies condition 1 or 2. This allows to determine a value of $G(t)$ and the corrisponding distribution over the wavenumber range.

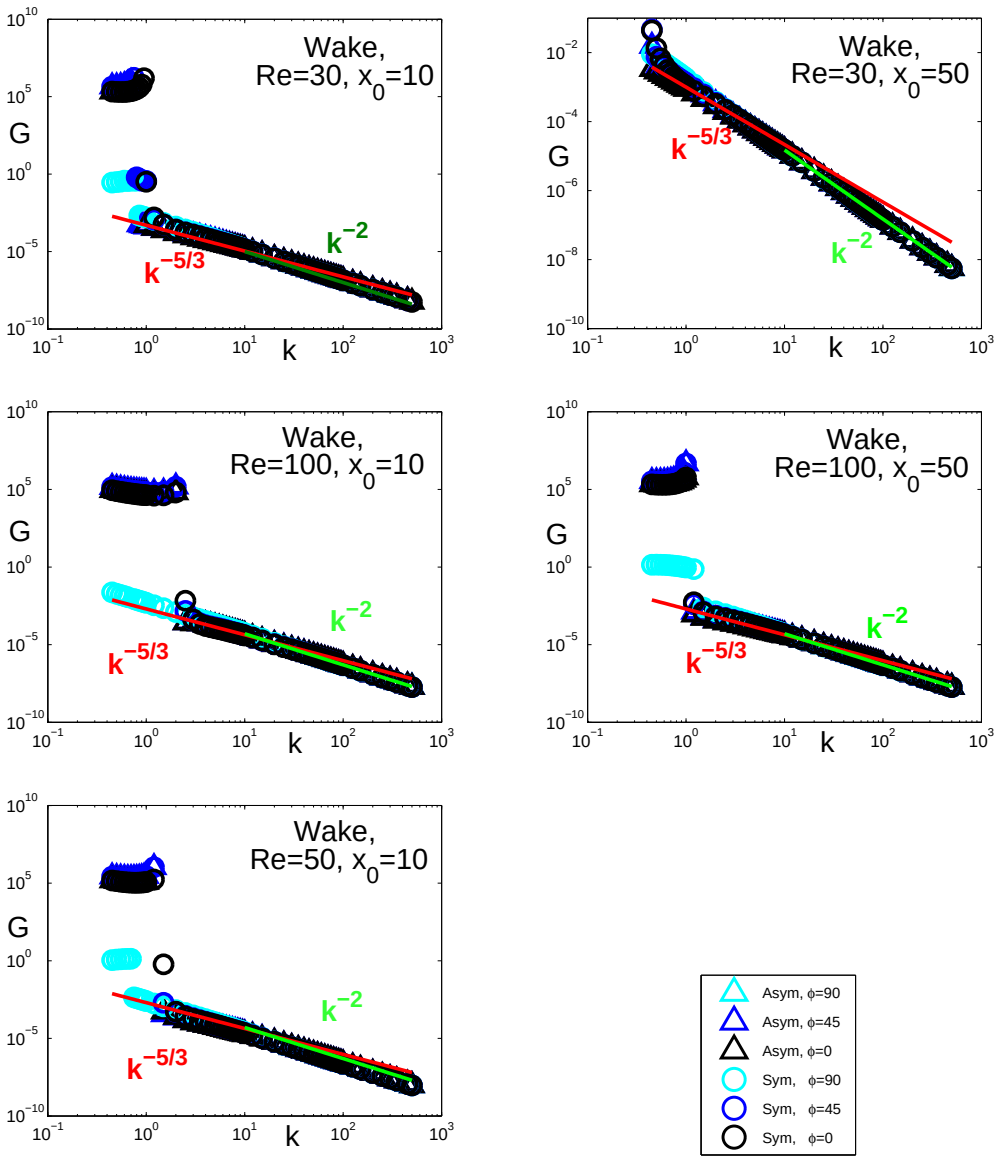

Figure 5.6: Energy spectrum.

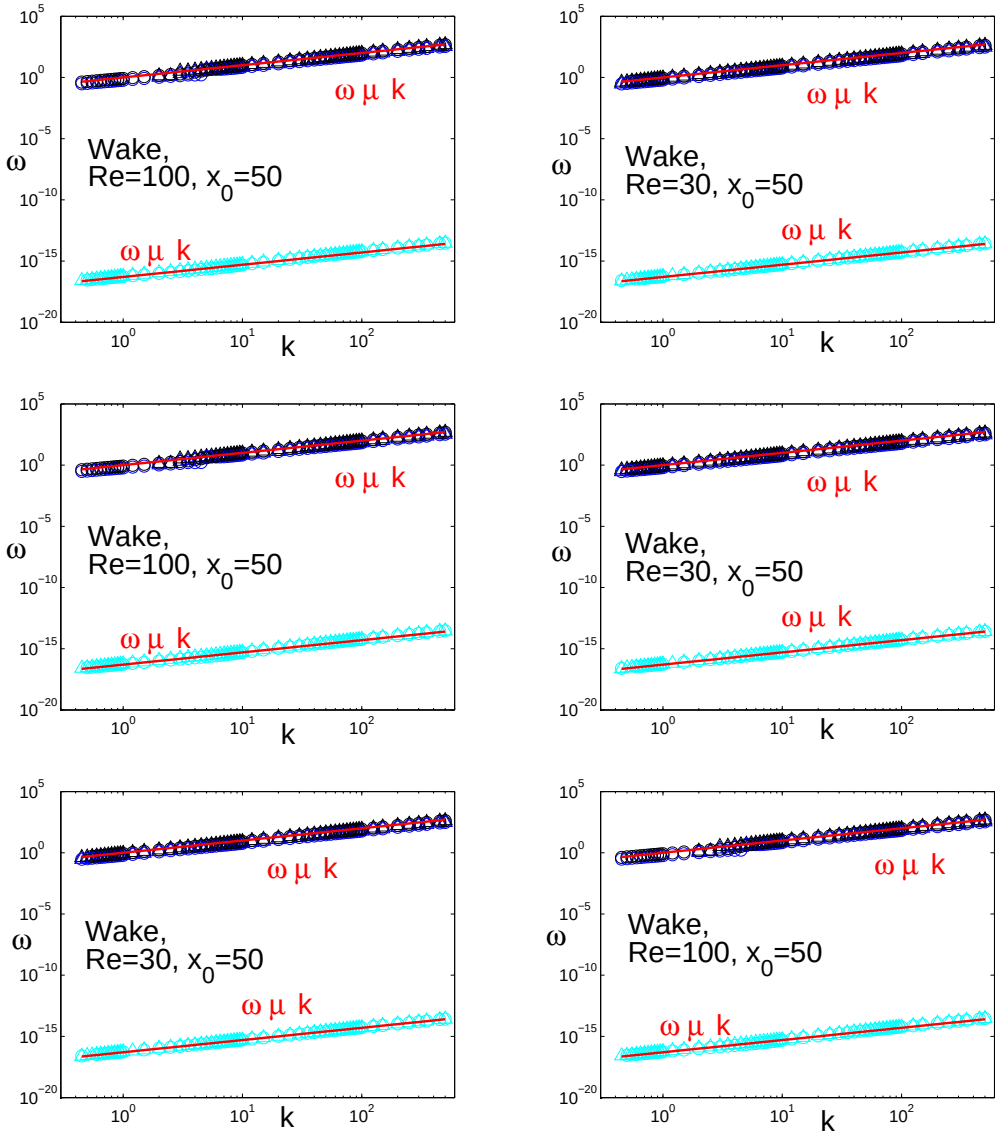

Figure 5.7: Frequency spectrum.

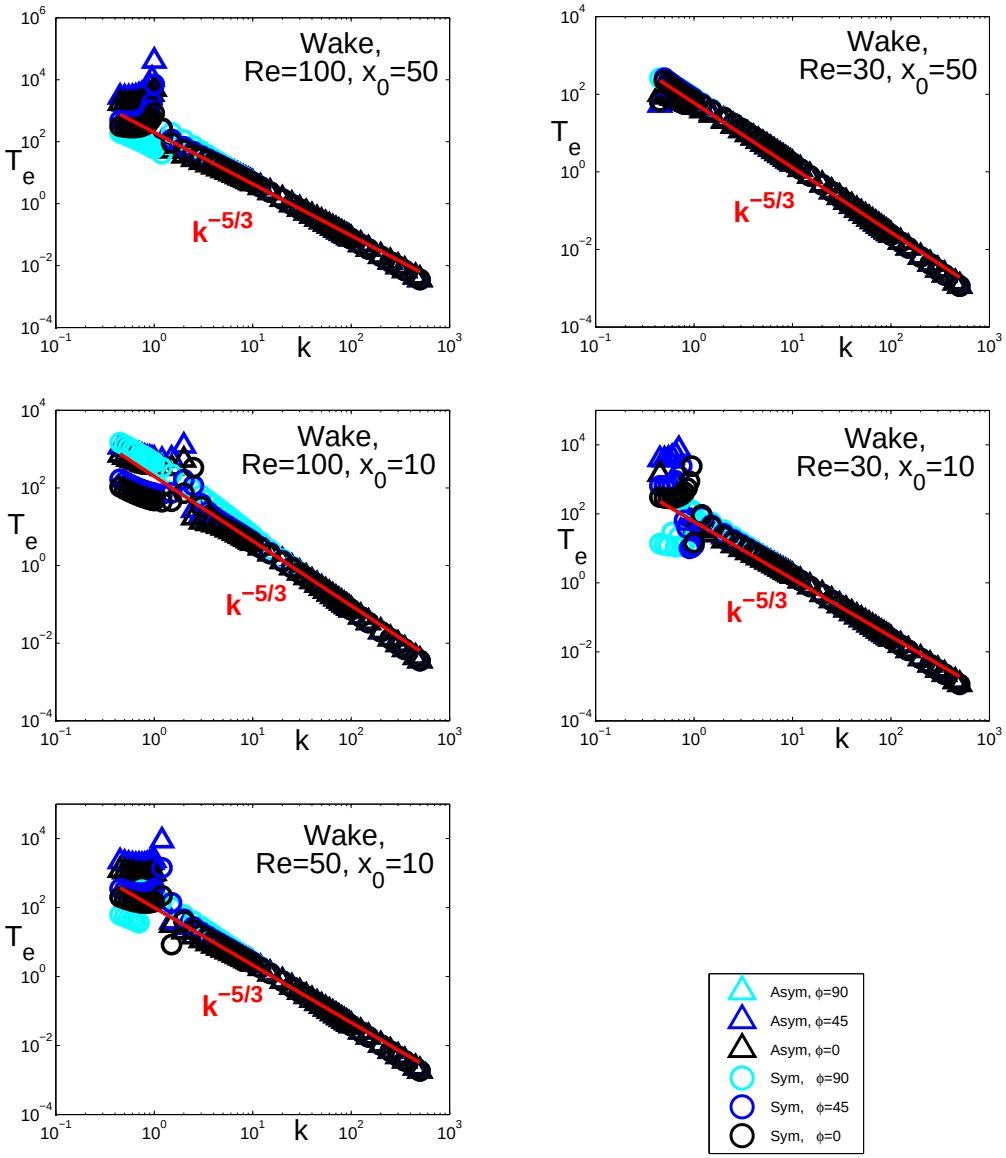

Figure 5.8: Time spectrum.

5.3 Collective behaviour of perturbations

The aim of the thesis is to see how much are important the non-linear terms in turbulence. The idea is to construct a turbulent flow by superposition of single waves with different wavenumber (the solutions of (4.7)), and then to study the flow so obtained with turbulence methods. Since equations (4.7) are linear, the superpositions principle holds. In other words, the sum of solutions is a solution. The principal feature of turbulence is randomness, so for this reason the superposition should be governed by a random law. This is done combining solutions using the MATLAB script `Collective_random_energy_behaviour` (that is explicitly written in Appendix A). The sum of perturbations is possible thanks to the script `Interpolated_velocity` that, fixed a value y_0 of y (in this case $y_0 = 0$), interpolate the velocity components on the same time instants.

In this work as been considered the case $Re = 30$, $x_0 = 50$ because for this set of parameters, all the wavenumbers presents a stable character. Considering a set of 34 wavenumbers (from $k = 3$ to $k = 100$), the two possible initial condition (symmetric/asymmetric) and five obliquity angles ($\phi = 0$, $\pi/4$, $\pi/2$, $-\pi/4$, $-\pi/2$), there are 340 waves that can be summed. Long waves ($k \in [3, 10]$) have a transient time that reach 50 time scale, while short waves ($k \in [15, 100]$) ends after 10 time scale. This means that short waves are faster than long waves. Furthermore short waves decades very quickly, so is difficult to notice their presence. In order to allow to see short waves a normalization of velocity components u, $v\,w$ has been made. The turbulent randomness has been simulated introducing two random parameters R, IT respectively

1. the time to enter into the collective system,

2. the time on the transient of the single wave that is taken as its starting point.

In such a way waves enters randomly in time and space (in the sense that can enter out of phase). When a wave finish its own transitory, can randomly enter again in the system because it takes two new random parameters R and IT. This method allow to sum waves on very long times, and not only on the longer transitory of the system (50 times scale).

In figure (5.9) the temporal evolution of the collective perturbative flow is shown. The other way to study the collective behaviour is visulizing the perturbative velocity component u, v, w and energy e as functions of spatial coordinates x and z, as shown in figure (a), (b) of (5.10). It is evident from

the two pictures of (5.10) the presence of long waves (k small) and short waves (k large).

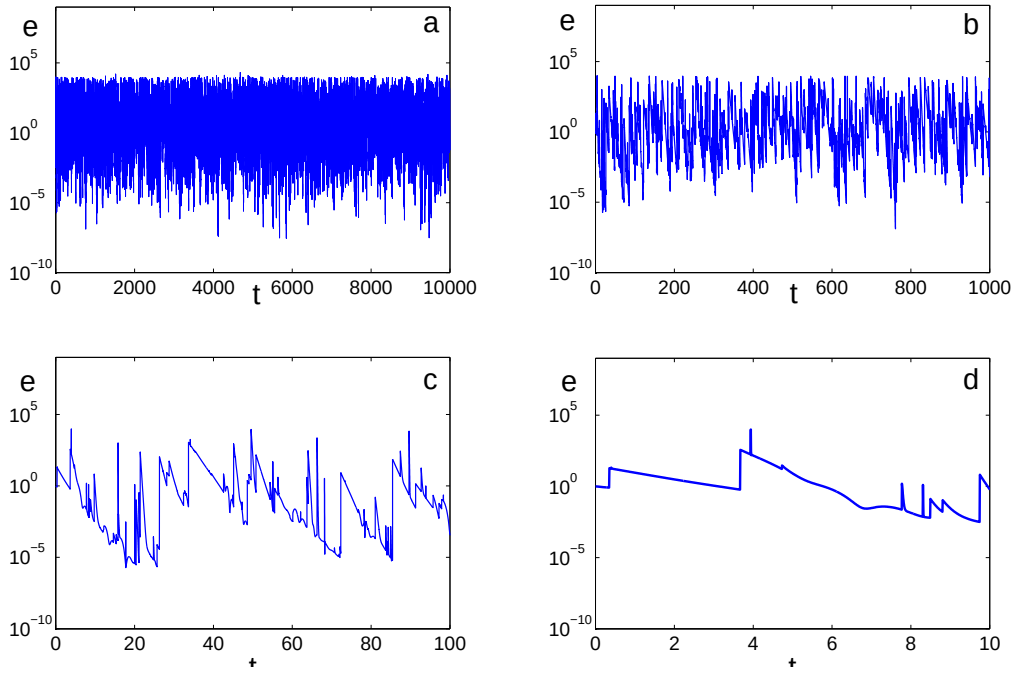

Figure 5.9: Collective perturbative energy evolution. The evolution time varies from $t = 0$ to $t = 10000$ time scales. The final time is taken large ($t = 10000$) in order to allow long waves to enter again in the system while their transient is finished (long waves last through 50 time scales). In figure (a) is presented the complete evolution. Figure (b), (c), (d) are enlargements of (a), respectively on 1000, 100, 10 time scales.

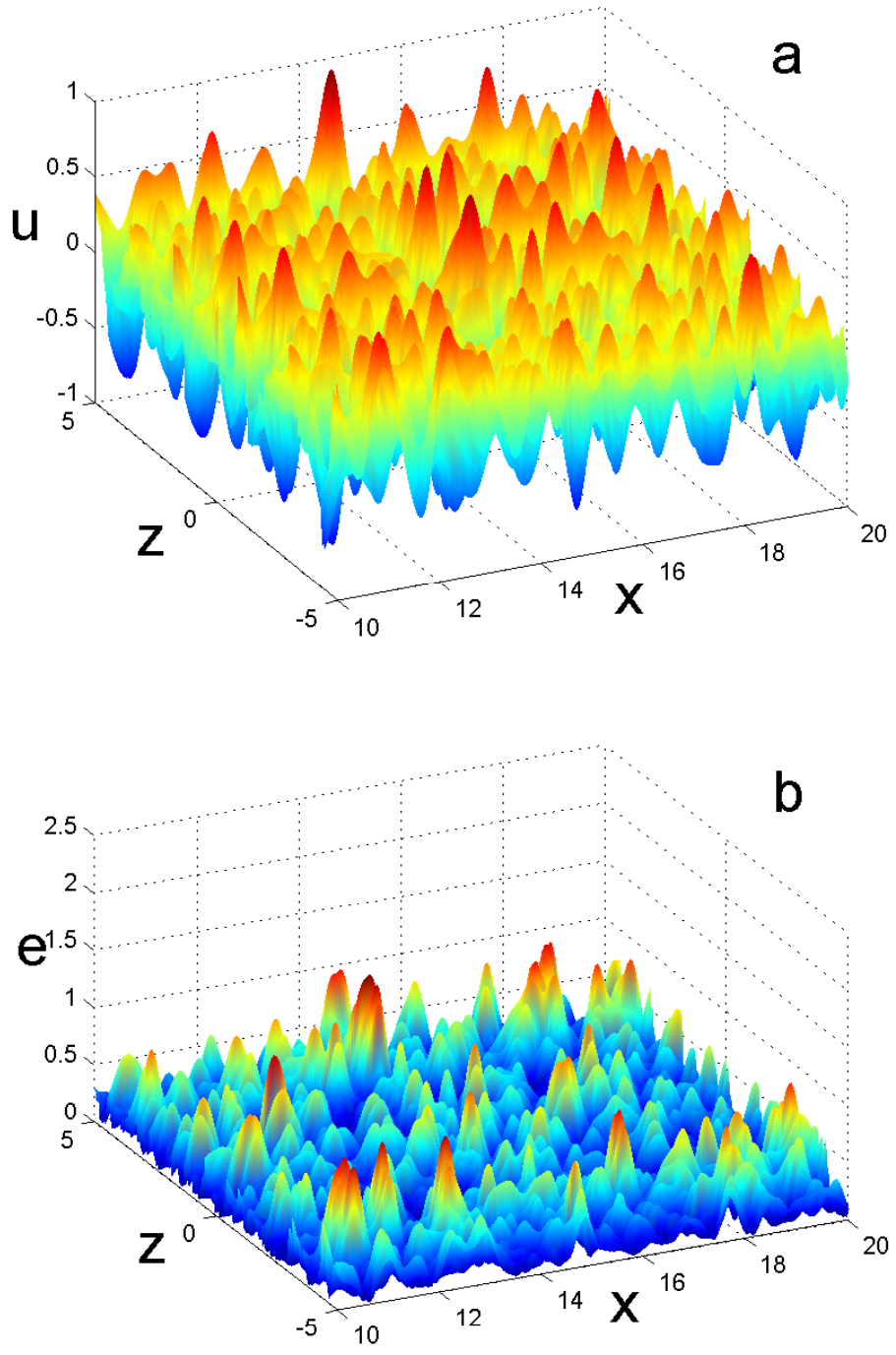

Figure 5.10: Collective behaviour. In figure (a) the collective $u(x, z)$ distribution is shown. In this picture are evident long (smooth waves) and short waves (peaked waves). In figure (b) the collective energy ditribution $e(x, z)$ is presented.

5.4 Conclusions

The experimental approach (based on the numerical determination of a large number of perturbations) here proposed to approximate the general solution of a Navier-Stokes field leads us to observe that, whether the waves are aligned with the same exponent $-5/3$ that is observed in the spectrum of the velocity fluctuation of fully developed turbulent flows, where the non linear interaction is considered dominant. At the moment, one can conclude that the spectral power-law scaling of intermediate/inertial waves (with an exponent close to $-5/3$) is a general dynamical property of the Navier-Stokes solutions which encompass the nonlinear interaction. A good ageement with experimental data.

Chapter 6

Code implementation and optimization

In this chapter numerical code features are presented. In order to solve problem (4.7), numerical codes has been developed using the software *Matlab*. A previous version of the routine has been optimized to obtain more efficiency in terms of computational velocity and memory exploit. Implemented codes are shown in Appendix A.

In section (6.1) numerical solutor for problem (4.7) is presented. The numerical scheme is reported and the reasons why this is the best method for this problem are explained.

In section (6.3) the optimization task is exposed. Code optimization involves the application of rules and algorithms to program code with the goal of making it faster, smaller, more efficient, and so on. Two classical tecniques has been used: *vectorization* and *array preallocation*. MATLAB is a high-level language and interactive environment that enables to perform computationally intensive tasks. It is a program that was originally designed to simplify the implementation of numerical linear algebra routines, so its easy to enter matrices and vectors, and manipulate them.

In section (6.4) code automation features are presented.

6.1 Ode solver

Solution of (4.7) has been found using the ODE solver `ode23`, that solve the equation

$$\mathbf{M}\,\mathbf{y}' = \mathbf{H}(\mathbf{x}, \mathbf{y}),$$

using the Bogacki-Shampine method. Since in this case matrix $\mathbf{M}$ is constant (in particular $\mathbf{M} = \mathbf{I}$) and problem (4.7) is moderately stiff, the best solver

is `ode23`.

A comparision between other methods has been done. In figure (6.1) is shown the energy grow factor $G(t)$ transitory obtained with different solvers. From this picture can be seen that `ode23` don't gives numerical oscillations that other solvers develop.

As said before, in Matlab solver `ode23`, the Bogacki-Shampine (Shampine & Reichelt 1997 [29]) method is implemented. The Bogacki-Shampine method, proposed by Przemyslaw Bogacki and Lawrence F. Shampine in 1989 (Bogacki & Shampine 1989 [5]), is a Runge-Kutta method of order three with four stages with the First Same As Last (FSAL) property, so that it uses approximately three function evaluations per step. It has an embedded second-order method which can be used to implement *adaptive step size*. Low-order methods are more suitable than higher-order methods like the Dormand-Prince method (implemented in solver `ode45`) of order five, if only a crude approximation to the solution is required. Bogacki and Shampine argue that their method outperforms other third-order methods with an embedded method of order two. Following the standard notation, the differential equation to be solved is $y^{'} = f(t, y)$. Furthermore, y_n denotes the numerical solution at time t_n and h_n is the step size, defined by $h_n = t_{n+1} - t_n$. Then, one step of the Bogacki-Shampine method is given by:

$$k_1 = f(t_n, y_n)$$

$$k_2 = f\left(t_n + \tfrac{1}{2}h_n,\, y_n + \tfrac{1}{2}hk_1\right)$$

$$k_3 = f\left(t_n + \tfrac{3}{4}h_n,\, y_n + \tfrac{3}{4}hk_2\right)$$

$$y_{n+1} = y_n + \tfrac{2}{9}hk_1 + \tfrac{1}{3}hk_2 + \tfrac{4}{9}hk_3$$

$$k_4 = f\left(t_n + h_n,\, y_{n+1}\right)$$

$$z_{n+1} = y_n + \tfrac{7}{24}hk_1 + \tfrac{1}{4}hk_2 + \tfrac{1}{3}hk_3 + \tfrac{1}{8}hk_4.$$

Here, y_{n+1} is a third-order approximation to the exact solution. The method for calculating y_{n+1} is due to Ralston (1965). On the other hand, z_{n+1} is a second-order approximation, so the difference between y_{n+1} and z_{n+1} can be used to adapt the step size. The FSAL property is that the stage value k_4 in one step equals k_1 in the next step; thus, only three function evaluations are needed per step.

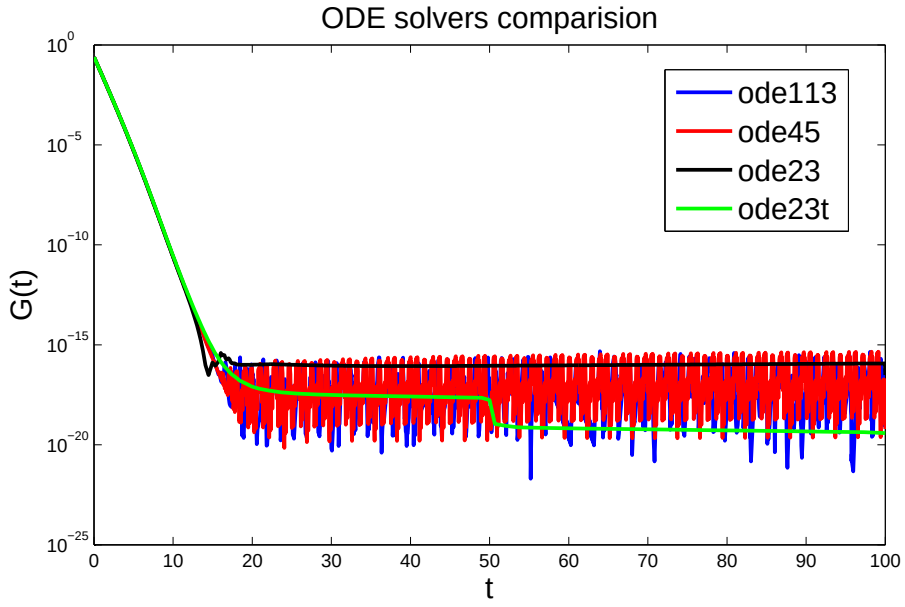

Figure 6.1: Comparision between Matlab solvers. In this picture the growth factor $G(t)$ of Re $= 100$, $x = 50$, asym, $\phi = \pi/4$, $k = 10$ has been calculated using different ode solvers. ode45 and ode113 presents a considerable numerical obscillation while ode23t gives numerical jumps.

6.2 Accuracy order of numerical derivatives

We also investigated how the choice of numerical method which approximates the derivative of the amplification factor affects the value of this slope. In Figure6.2 is shown dG/dt computed by finite difference of different order:

- 2nd order accuracy,
$$dg_i = \frac{g_{i+1} - g_{i-1}}{t_{i+1} - t_{i-1}}$$
- 4th order accuracy
$$dg_i = \frac{g_{i-2} - 9g_{i-1} + 9g_{i+1} - g_{i+2}}{t_{i+6} - t_{i-6}}$$
- 6th order accuracy
$$dg_i = \frac{-g_{i-3} + 9g_{i-2} - 45g_{i-1} + 45g_{i+1} - 9g_{i+2} + g_{i+3}}{t_{i+30} - t_{i-30}}$$

The comparison among the methods is made for a large ($k = 1$) and an inertial ($k = 10$) wave, at high Reynolds number ($Re = 100$), intermediate field wake configuration ($x_0 = 10$) and symmetric input. The three finite differences seems completely equivalent, thus for simplicity we will use always the second order one. The last question is about the ranges classification.

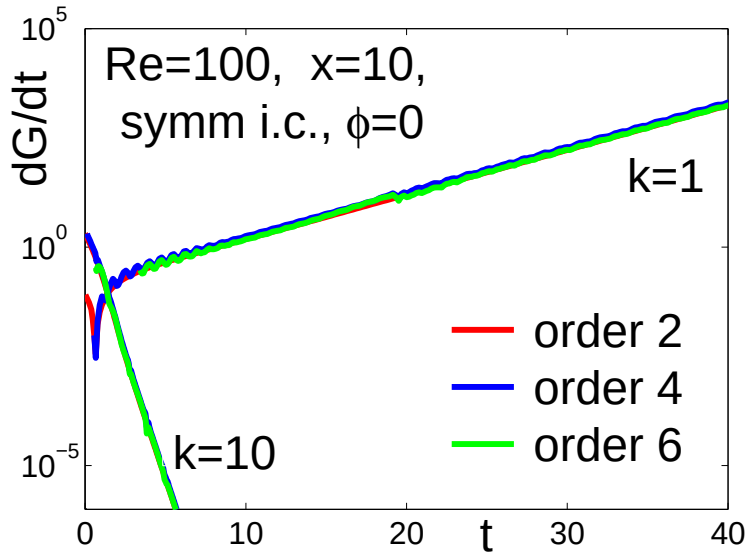

Figure 6.2: Comparison between derivative of amplification factor obtained by finite difference with different accurancy.

We want investigate how our classification criterion of long-inertial and dissipative range affects the the slopes computation. It is thus considered the two very different configurations (represented in figure (6.3)) and computed the slopes of the spectrum in the three ranges, varying slightly the extremes that define them.

Long Range	$\phi = 0$	$\phi = 0$
$0.45 \leq k \leq 1$	-0.8828	-1.9549
$0.5 \leq k \leq 0.95$	-0.8623	-1.9555
$0.55 \leq k \leq 0.9$	-0.8592	-1.9592
$0.45 \leq k \leq 1.2$	-0.8177	-1.9476
std	0.0273	0.0182

Inertial Range	$\phi = 0$	$\phi = 90$
$3.5 \leq k \leq 50$	-1.8144	-2.0133
$3 \leq k \leq 55$	-1.8538	-2.0685
$4 \leq k \leq 45$	-1.8025	-1.9990
$4.5 \leq k \leq 40$	-1.7841	-2.0107
std	0.0295	0.0310

Table 6.1: Energy spectrum slope. Long and inertial range

Dissipative Range	$\phi = 0$	$\phi = 90$
$50 \leq k \leq 500$	-2.0890	-2.0493
$55 \leq k \leq 450$	-2.0471	-2.0659
$60 \leq k \leq 350$	-2.0381	-2.0281
$65 \leq k \leq 300$	-1.9978	-2.0685
std	0.0244	0.00186

Table 6.2: Energy spectrum slope

Varying slightly the definition of the three ranges one obtain the slopes summarized in tables 6.2 and 6.2, where *std* is the standard deviation. Can be observed that the percentage error is between 1.82% and 3.1% that is an acceptable error bar.

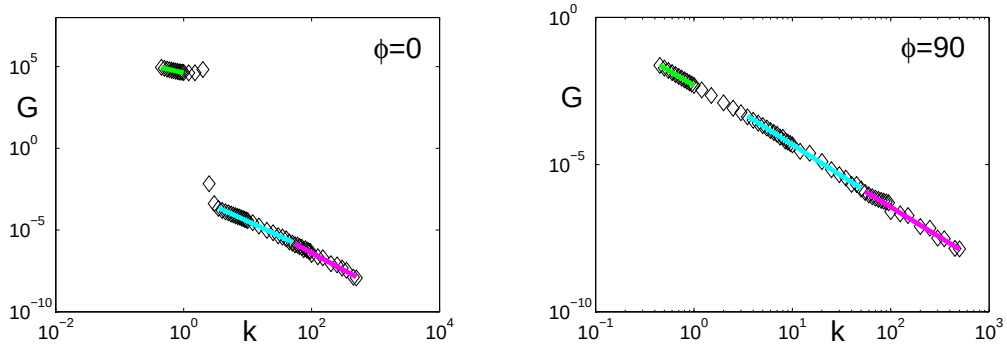

Figure 6.3: Energy spectrum obtained at high Reynolds number ($Re = 100$), intermediate field wake ($x_= = 10$), symmetric initial condition longitudinal (on the left) and transversal (on the right) waves. Green, magenta and cyan line indicate long, inertial and dissipative ranges defined as in the first lines of tables 6.2 and 6.2.

6.3 Optimization

Optimization is the process of transforming a piece of code to make more efficient (either in terms of time or space) without changing its output or side-effects. The only difference visible to the code's user should be that it runs faster and/or consumes less memory. Since Matlab 5.0, a tool called *profiler* helps determine where the bottlenecks are in a program. Using the profiler one can identify which functions in the code consume the most time, and so where the optimizing techniques can be applied. The techniques used, *vectorization* and *array preallocation*, are presented in section (6.3.1) and (6.3.2) respectively. To show optimizaton improvement, a speed-up analysis on numerical code for problem (4.7) has been done. In figure (6.4) the mean ratio of the computing times T_{no} and T_o (respectively non-optimized and optimized time), for different wavenumbers k is shown. From figure (6.4) can be observed that optimized code produce outputs at least 11 times faster than non-optimized code. In conclusion, whenever the speed of MATLAB code is important, optimization is fundamental.

6.3.1 Array preallocation

Though MATLAB will automatically adjust the size of a matrix (or vector) it is usually a good idea to preallocate the matrix. Preallocation incurs the cost of memory allocation just once, and it guarantees that matrix elements will be stored in contiguous locations in RAM (by columns). The `for` and `while` loops that incrementally increase, or grow, the size of a data structure each time through the loop can adversely affect performance and memory use. For example consider the following code that creates a scalar variable x, and then gradually increases the size of x in a for loop instead of preallocating the required amount of memory at the start

```
x = 0;
for k = 2:1000
   x(k) = x(k-1) + 5;
end
```

Changing the first line to preallocate a 1-by-1000 block of memory for x initialized to zero there is no need to repeatedly reallocate memory and move data as more values are assigned to x in the loop

```
x = zeros(1, 1000);
for k = 2:1000
   x(k) = x(k-1) + 5;
end
```

Repeatedly resizing arrays often requires that MATLAB spend extra time looking for larger contiguous blocks of memory and then moving the array into those blocks. Code execution can be improved on time by preallocating the maximum amount of space that would be required for the array ahead of time. Perhaps a more important benefit is avoiding fragmentation. If the entire data object is allocated together rather than in small pieces, freeing it will definitely return usable contiguous space of the entire size to the free memory pool to be used by later allocations. On the other hand, if you allocate each small piece separately, there's a good possibility that they won't be contiguous.

6.3.2 Vectorization

The power of Matlab is that can manipulate matrices as a whole, so to improve code speed is necessary to eliminate loops where there are element-by-element operations. This technique, known as *vectorization*, allow to exploit Matlab skills at best. The MATLAB software uses a matrix language, which means it is designed for vector and matrix operations. Vectorization means converting `for` and `while` loops to equivalent vector or matrix operations. A simple example of vectorization can be made by considering the non-vectorized code

```
i = 0;
for t = 0:.01:10
    i = i + 1;
    y(i) = sin(t);
end
```

and the vectorized version of the same code

```
t = 0:.01:10
y = sin(t);
```

The second script executes much faster than the first and is the way MATLAB is meant to be used. Vectorization is often a smooth process; however, in many specific cases, it can be difficult to construct a vectorized routine. The speed of a numerical algorithm in MATLAB is very sensitive to whether or not vectorized operations are used.

6.4 Code automation

Another code improvement has been done implementing an automatic change of simulation's parameters, and a dynamic generation of folders and

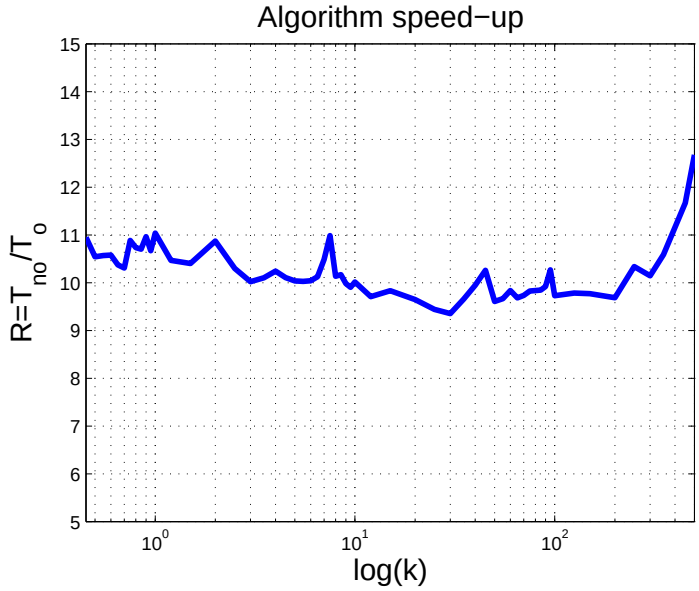

Figure 6.4: Algorithm speed-up. Times $T_{no}\,, T_o$ are respectively the computational times of non-optimized and optimized code, k is the wavenumber. From this figure is clear that in mean optimized code runs 10 times faster than non-optimized one.

files names. The idea is to change parameters with loop cycles. At every loop the code take new parameters from arrays (where parameters are stored). When a simulation is finished the code continue with the next, until all the parameters are used. This strategy allow to avoid to waste time with a manual parameter change, and more important, the code can indipendently run for all the parameters without help. In other words one don't have to continuously follow the code waiting to launch the next simulation.

When the code is running, folders and files are created and organized into a hierarchy tree structure, following the level order

$$Re \rightarrow x \rightarrow sym/asym \rightarrow \phi \rightarrow k.$$

Text files containing the solution are stored into "leaf" folders at level k. An example of filenames are reported below

```
Re_100_x_50_asym_phi_45_k_8.5_u_1.txt
Re_100_x_50_asym_phi_45_k_8.5_v_1.txt
Re_100_x_50_asym_phi_45_k_8.5_w_1.txt
Re_100_x_50_asym_phi_45_k_8.5_t_1.txt
Re_100_x_50_asym_phi_45_k_8.5_omega_y_1.txt
Re_100_x_50_asym_phi_45_k_8.5_energy_1.txt
```

At every loop, file and folder names are made by converting in string format and concatenating the new parameters. Code automation really can make a difference especially when it comes to reducing human errors and improving work speed. To see explicitly how this is done see Appendix A.

6.5 Perturbative solution data-base

All the simulation's output files are stored into a on-line disk, that can be found at IP address 130.192.25.166. The data-base's organization is analogous to the hierarchy tree structure described in section (6.4). Furthermore, using an FTP client is easy to download files from the disk.

Appendix A

Matlab code

In order to solve problem (4.7), numerical codes has been developed. The code has been implemented using the software *Matlab*. A previous version of the routine has been optimized to obtain more efficiency in terms of computational velocy and memory exploit.

A.1 Launch in sequence

Defined the parameters, the routine `Launch_in_sequence` allow to launch simulations. Every simulation ends when the asymptotic conditions is satisfied, and when this condition is reached the program make an automatic parameters change in order to continue with the next simulation.

```
%                              Launch_in_sequence

close all
clear all
global x R phi alpha xx rr ss gg dd alpha_i alpha_r ALPHA gamma beta0 eps T0
global h h2 y0 y N v0 omega0 U dU_dy d2U_dy2 A
global CondIniz CR OR CurrentRun out simulationfolder tend tlim m
disp('-----------------------------------------------')
disp('Launch in sequence')
% Phisical parameters of simulation
R    = 30;      % 30 50 100
x    = 10;      % 10 50
phi  = pi/4;    % 0 pi/4 pi/2
grad = 45;      % 0 45 90
ss   = 'asym';  % sym o asym

% Variable for directory and files name
rr = num2str(R);
xx = num2str(x);
gg = num2str(grad);
% Define the name of simulation's directory
simulationfolder = ['D:\simulazioni\Transient_simulation
                    \Re_' rr '_x_' xx '\Re_' rr '_x_' xx '_' ss '\Re_' rr '_x_' xx '_' ss '_phi_' gg];
% Polar wavenumbers
```

```
kappa = [0.45 0.5 0.55 0.6 0.65 0.7 0.75 0.8 0.85 0.9 0.95 1 1.2 1.5 2,2.5 3...
         3.5 4 4.5 5 5.5 6 6.5 7 7.5 8 8.5 9 9.5 10 12 15 20 25 30 35 40 45 ...
         50 55 60 65 70 75 80 85 90 95 100 125 150 200 250 300 350 450 500];
C_1   = 1.22 + 0.000067*(R^2);
eps   = 1/R;
h     = 0.05;
h2    = h^2;
y0    = 0;
beta0 = 1;
for i=1:6
    IND = [1 6]*(i==1)+[7 12]*(i==2)+[13 16]*(i==3)+[17 31]*(i==4)+[32 49]*(i==5)+[50 58]*(i==6);
    T0  = 200*(i==1)+200*(i==2)+100*(i==3)+50*(i==4)+10*(i==5)+2*(i==6);
    Y   = [-40 40]*(i==1)+[-30 30]*(i==2)+[-20 20]*(i>=3);
    y   = Y(1):h:Y(2);
    for m=IND(1):IND(2)
        alpha   = kappa(m);
        dd      = num2str(alpha);
        alpha_r = alpha*cos(phi);
        alpha_i = 0.0;
        gamma   = alpha*sin(phi);
        ALPHA   = alpha^2 - alpha_i^2 + 2*1i*alpha_r*alpha_i;
        N       = length(y);
        % Base flow
        U       = 1 - 1/sqrt(x)*C_1*exp(-0.25*R*y.^2/(x));
        dU_dy   = 0.5/sqrt(x)*C_1*R/x*y.*exp(-0.25*R*y.^2/(x));
        d2U_dy2 = 0.5/sqrt(x)*C_1*R/x*exp(-0.25*R*y.^2/(x))-...
                  0.25/sqrt(x)*C_1*(R*y/x).^2.*exp(-0.25*R*y.^2/(x));
        % Construction of the Laplacian Matrix A and call ode113 to solve evolutive
        % equations for Gamma and omega_y. Solution vector is u_sol=[Gamma omega_y]
        d2          = 1/h2*ones(N,1)*[1 -2 1];
        d2(1,2)     = 0;   d2(2,3)     = 0;   d2(end-1,1) = 0;      d2(end,2)   = 0;
        % matrix for computing laplacian (with Robin boundary conditions).
        d2          = d2+-ALPHA*ones(N,1)*[0 1 0];
        d2(1,2)     = -sqrt(ALPHA)+-1/h;
        d2(2,3)     = 1/h;  d2(end-1,1) = -1/h;   d2(end,2)   = sqrt(ALPHA)+1/h;
        A           = spdiags(d2, -1:1, N, N);
        jjj    = 1; %<----------------------- n Current Run
        out    = 0;
        tend   = 0;
        tlim   = 1600;
        v0     = [];
        omega0 = [];
        while (out==0 && tend<=tlim )
            CondIniz = 1;
            if jjj==1
                CondIniz = 0;
            end
            tend = T0*jjj;
            disp('-------------------------------------------------')
            InformazionRun = ['Run n ' num2str(jjj) '  Re= ' rr ' x= ' xx
                              ' ' ss ' phi= ' gg ' k= ' num2str(alpha)];
            disp(InformazionRun)
            disp(['tend= ' tend])
            CurrentRun = jjj;
            OldRun     = CurrentRun-1;
            CR         = num2str(CurrentRun);
            OR         = num2str(OldRun);
            IVP_completo
            jjj = jjj+1;
        end
    end
end
```

A.2 IVP completo

In the routine `IVP_completo` the equations system (4.7) is solved. This program uses the subrutines `dhdt_vettorizzato`, `solve_for_v_complete` and, to check if the asymptotic condition, the routine `Check_asymptotic_condition`. The outputs are the fourier-transformed velocity field components $\hat{u}, \hat{v}, \hat{w}$, the fourier-transformed vorticity $\hat{\omega}_y$, the time and energy evolution. All the outputs are saved into *.txt* files.

```
%                            IVP_completo
%                    solve_complete + velocity_field

% Complete initial-value problem (Scarsoglio, Tordella & Criminale, Stud.
% Applied Math. 2009) Energy spectrum Longitudinal Base Flow U=U(y;x0,R)
% Calls dhdt and solve_for_v_complete



global out

disp('IVP_completo')
tic
format long
foldername = ['\Re_' rr '_x_' xx '_' ss '_phi_' gg '_k_' dd];
% Initial conditions
disp('Inizialization...')
tic
if(CondIniz==0)
    disp('.....from function...')
    tinit = 0;
    if(strcmp(ss, 'sym'))
        % even disturbance-sym
        Gamma0 = (exp(-(y-y0).^2).* (4*beta0*(y-y0).*sin(beta0*(y-y0))+cos(beta0*(y-y0)).*...
                 (-beta0^2-2+4*(y-y0).^2))-ALPHA*exp(-(y-y0).^2).*cos(beta0*(y-y0)));
    else
        % odd disturbance-asym
        Gamma0 = (exp(-(y-y0).^2).*(-4*beta0*(y-y0).*cos(beta0*(y-y0))+sin(beta0*(y-y0)).*...
                 (-beta0^2 -2 +4*(y-y0).^2))-ALPHA*exp(-(y-y0).^2).*sin(beta0*(y-y0)));
    end
    omega0 = zeros(1,N);
    init   = [Gamma0,omega0];
else
    filename_t = [simulationfolder foldername
                 '\Re_' rr '_x_' xx '_' ss '_phi_' gg '_k_' dd '_t_' OR '.txt'];
    fid = fopen(filename_t, 'r');
    T1  = fscanf(fid,'%f', [1 inf]);
    fclose(fid);
    tinit = T1(length(T1));
    if (isempty(v0)==1)
        disp('.........from file...')
        Gamma0     = zeros(1,N);
        foldername = ['\Re_' rr '_x_' xx '_' ss '_phi_' gg '_k_' dd];
        filename2  = [simulationfolder foldername
                      '\Re_' rr '_x_' xx '_' ss '_phi_' gg '_k_' dd '_v_' OR '.txt'];
        filename4  = [simulationfolder foldername
                      '\Re_' rr '_x_' xx '_' ss '_phi_' gg '_k_' dd '_omega_y_' OR '.txt'];
        fid2 = fopen(filename2, 'r');
        V1   = fscanf(fid2,'%f', [2 length(T1)*N]);
        fclose(fid2);
```

```
        fid4   = fopen(filename4, 'r');
        OMEGA1 = fscanf(fid4,'%f', [2 length(T1)*N]);
        fclose(fid4);
        j = (length(T1)-1)*N+1:(length(T1)-1)*N+N;
        v0     = V1(1,j)+1i*V1(2,j);
        omega0 = OMEGA1(1,j)+1i*OMEGA1(2,j);
        clear T1 V1 OMEGA1
    else
        disp('v0, omega0 taken from previous Run')
    end
    Gamma0 = ([v0(1),v0(1:N-2),v0(N-2)]-2*[v0(2),v0(2:N-1),v0(N-1)]+[v0(3),v0(3:N),v0(N)])/h2-ALPHA*v0;
    init   = [Gamma0,omega0];
end
filename1 = [simulationfolder foldername
            '\Re_' rr '_x_' xx '_' ss '_phi_' gg '_k_' dd '_u_' CR '.txt'];
filename2 = [simulationfolder foldername
            '\Re_' rr '_x_' xx '_' ss '_phi_' gg '_k_' dd '_v_' CR '.txt'];
filename3 = [simulationfolder foldername
            '\Re_' rr '_x_' xx '_' ss '_phi_' gg '_k_' dd '_w_' CR '.txt'];
filename4 = [simulationfolder foldername
            '\Re_' rr '_x_' xx '_' ss '_phi_' gg '_k_' dd '_omega_y_' CR '.txt'];
filename5 = [simulationfolder foldername
            '\Re_' rr '_x_' xx '_' ss '_phi_' gg '_k_' dd '_energy_' CR '.txt'];
filename_t= [simulationfolder foldername
            '\Re_' rr '_x_' xx '_' ss '_phi_' gg '_k_' dd '_t_' CR '.txt'];
% make simulation storage directory
[~,~,~] = mkdir(simulationfolder,foldername);
toc
disp('Inizialized!')
disp('Solve equation for omega_y e Gamma...')
[t,u_sol] = ode23('dhdt_vettorizzato',[tinit tend],init);
toc
disp('Solve for u v w e...')
tic
fid1 = fopen(filename1,'w');
fid2 = fopen(filename2,'w');
fid3 = fopen(filename3,'w');
fid4 = fopen(filename4,'w');
fide = fopen(filename5,'w');
fid_t= fopen(filename_t,'w');
e = zeros(1,1);
s = N+1:2*N;
for j=1:length(t)
    % Solution of the Laplacian (call solve_for_v_complete) and output omega_y v
    v = solve_for_v_complete(u_sol(j,:).');
    v = v.';
    omega_y = u_sol(j,s);

    u  = (-(alpha_r+1i*alpha_i)*([v(2:N),v(N)]-[v(1:N-1),v(N-1)])/h+gamma*omega_y)/(1i*ALPHA);

    w  = (-gamma*([v(2:N),v(N)]-[v(1:N-1),v(N-1)])/h-(alpha_r+1i*alpha_i)*omega_y)/(1i*ALPHA);

    ke = abs(u).^2+abs(v).^2+abs(w).^2;

    e(j) = trapz(y,ke);
    outputu = [real(u); imag(u)];
    fprintf(fid1,'%d    %d\n',outputu);
    outputv = [real(v); imag(v)];
    fprintf(fid2,'%d    %d\n',outputv);
    outputw = [real(w); imag(w)];
    fprintf(fid3,'%d    %d\n',outputw);
    outputomega = [real(omega_y); imag(omega_y)];
```

```
    fprintf(fid4,'%d    %d\n',outputomega);
    outpute = [t(j); e(j)];
    fprintf(fide,'%d    %d\n',outpute);
    fprintf(fid_t,'%d\n', t(j));
end
fclose(fid1);
fclose(fid2);
fclose(fid3);
fclose(fid4);
fclose(fide);
fclose(fid_t);
toc
out    = 0;
out    = verifica_condizione(m,e,t,rr,xx,ss,gg,dd,foldername,simulationfolder,CurrentRun,out);
v0     = v;
omega0 = omega_y;
clear u_sol t e v omega_y
```

A.3 dhdt vettorizzato

```
%                         dh_dt_vettorizzato
% Right-hand-side of evolutive equations for Gamma (H) and omega (H1)



function H = dhdt_vettorizzato(~,u_sol)

global  N alpha alpha_i h2 U dU_dy d2U_dy2 phi eps ALPHA

u_sol(1) = 0;
u_sol(N) = 0;
v     = solve_for_v_complete(u_sol);
v     = v.';
H(1)  = 0;
H(N)  = 0;
H1(1) = 0;
H1(N) = 0;
u_sol = u_sol.';
s     = N+1:2*N;


H(2:N-1)  = -1i*alpha*U(2:N-1).*u_sol(2:N-1)*cos(phi)+1i*alpha*d2U_dy2(2:N-1).*v(2:N-1)*cos(phi)+...
            alpha_i*U(2:N-1).*u_sol(2:N-1)-alpha_i*d2U_dy2(2:N-1).*v(2:N-1)+...
            eps*((u_sol(1:N-2)-2*u_sol(2:N-1)+u_sol(3:N))/h2-ALPHA*u_sol(2:N-1));

H1(2:N-1) = -1i*alpha*sin(phi)*dU_dy(2:N-1).*v(2:N-1)-1i*alpha*cos(phi)*U(2:N-1).*u_sol(s(2):s(end)-1)+...
            alpha_i*U(2:N-1).*u_sol(s(2):s(end)-1)+ eps*((u_sol(s(1):s(end)-2)-2*u_sol(s(2):s(end)-1)+...
            u_sol(s(3):s(end)))/h2-ALPHA*u_sol(s(2):s(end)-1));
H = [H H1];
H = H.';
return
```

A.4 Solve for v complete

```
%                        solve_for_v_complete
% Solve Laplacian(v)=Gamma


function v = solve_for_v_complete(u_sol)

global  N A
u_sol([1 N]) = 0;
u_aux        = u_sol(1:N);
v            = A\u_aux;
return
```

A.5 Check asymptotic condition

```
%                       Check_asymptotic_condition


function out = verifica_condizione(m,e,t,rr,xx,ss,gg,dd,foldername,simulationfolder,CurrentRun,out)
tr = 0;
if CurrentRun==1
    e0 = e(1);
else
    file_e0 = [simulationfolder foldername '\Re_' rr '_x_' xx '_' ss '_phi_' gg '_k_' dd '_energy_1.txt'];
    fid1    = fopen(file_e0,'r');
    res_ene = fscanf(fid1,'%f', [2 1]);
    fclose(fid1);
    e0 = res_ene(2);
end
g      = e/e0;
dg     = [g(3:end)-g(1:end-2)]./[t(3:end)-t(1:end-2)];
tau_g  = g./dg;
t_norm = t./tau_g;

CS = find((m>=tr).*(t_norm>=3).*((dg<1e-4)+(dg>1e+4))~=0);
CI = find((m<tr).*(dg<1e+4)~=0);
if isempty(CS)
     if isempty(CI)
         disp(['k= ' dd ' condition not satisfied']);
     else
         k   = CI(1);
         T   = t(k);
         E   = e(k);
         out = 1;
         disp(['k= ' dd ' condition ok: E=' num2str(E) '  T=' num2str(T)]);
         disp('-----------------------------------------------')
     end
else
     k   = CS(1);
     T   = t(k);
     E   = e(k);
     out = 1;
     disp(['k= ' dd ' condition ok: E=' num2str(E) '  T=' num2str(T)]);
     disp('-----------------------------------------------')
end
return
```

A.6 Interpolated velocity

The routine `Interpolated_velocity` is a postprocessing routine. To study the collective behaviour the perturbations should be summed. Since the ode solver uses a variable time step, to sum perturbation velocity fields is necessary to interpolate the solutions over common time instants. Fixed a value y_0 on the y axis, the script `Interpolated_velocity` interpolate the velocity field components $u(t, x, y_0, z)$, $v(t, x, y_0, z)$, $w(t, x, y_0, z)$ on time.

```
%                       Interpolated_velocity


close all
clear all
rr    = '30';
xx    = '50';
S     = {'sym' 'asym'};
A     = {'0' '45' '90'};
phi   = [0 pi/4 pi/2];
h     = 0.05;
y     = -20:h:20;
N     = length(y);
y0    = 0;
I     = find(y==y0);
kappa = [0.45 0.5 0.55 0.6 0.65 0.7 0.75 0.8 0.85 0.9 0.95 1 1.2 1.5 2,2.5 3...
         3.5 4 4.5 5 5.5 6 6.5 7 7.5 8 8.5 9 9.5 10 12 15 20 25 30 35 40 45 ...
         50 55 60 65 70 75 80 85 90 95 100 125 150 200 250 300 350 450 500];
for i=1:2
    ss = S{i};
    for a=1:3
        gg = A{a};
        simulationfolder = ['D:\simulazioni\Transient_simulation\Re_' rr '_x_' xx
                            '\Re_' rr '_x_' xx '_' ss '\Re_' rr '_x_' xx '_' ss '_phi_' gg];
        main_folder = 'D:\simulazioni\Interpolated_velocity_y0_linear';
        for k=17:50
            tic
            alpha = kappa(k);
            dd    = num2str(alpha);
            foldername = ['\Re_' rr '_x_' xx '_' ss '_phi_' gg '_k_' dd];
            flag = 0;
            z  = 1;
            zz = num2str(z);
            folder_vel = ['\Re_' rr '_x_' xx '_' ss '_phi_' gg '\Re_' rr '_x_' xx '_' ss '_phi_' gg '_k_' dd];
            [~,mess,messid] = mkdir(main_folder,folder_vel);
            fileT = ['\Re_' rr '_x_' xx '_' ss '_phi_' gg '_k_' dd '_t_' zz '.txt'];
            fileU = ['\Re_' rr '_x_' xx '_' ss '_phi_' gg '_k_' dd '_u_' zz '.txt'];
            fileV = ['\Re_' rr '_x_' xx '_' ss '_phi_' gg '_k_' dd '_v_' zz '.txt'];
            fileW = ['\Re_' rr '_x_' xx '_' ss '_phi_' gg '_k_' dd '_w_' zz '.txt'];
            filename6 = [simulationfolder foldername fileT];
            filename7 = [simulationfolder foldername fileU];
            filename8 = [simulationfolder foldername fileV];
            filename9 = [simulationfolder foldername fileW];
            file_u = ['\Re_' rr '_x_' xx '_' ss '_phi_' gg '_k_' dd '_u_int.txt'];
            file_v = ['\Re_' rr '_x_' xx '_' ss '_phi_' gg '_k_' dd '_v_int.txt'];
            file_w = ['\Re_' rr '_x_' xx '_' ss '_phi_' gg '_k_' dd '_w_int.txt'];
            filename1 = [main_folder folder_vel file_u];
            filename2 = [main_folder folder_vel file_v];
```

```
            filename3 = [main_folder folder_vel file_w];
            fid = fopen(filename6,'r');
            t1  = fscanf(fid,'%f', [1 10000]);
            fclose(fid);
            nt   = length(t1);
            nvel = nt*N;
            fid  = fopen(filename7,'r');
            U    = fscanf(fid,'%f',[2 nvel]);
            fclose(fid);
            fid = fopen(filename8,'r');
            V   = fscanf(fid,'%f',[2 nvel]);
            fclose(fid);
            fid = fopen(filename9,'r');
            W   = fscanf(fid,'%f', [2 nvel]);
            fclose(fid);
            t   = t1(1):0.0065:t1(length(t1));

            s  = (0:length(t1)-1)*N+I;
            v1 = V(1,s)+1i*V(2,s);
            u1 = U(1,s)+1i*U(2,s);
            w1 = W(1,s)+1i*W(2,s);

            u  = interp1(t1,u1,t,'linear');
            v  = interp1(t1,v1,t,'linear');
            w  = interp1(t1,w1,t,'linear');
            fid1 = fopen(filename1,'wt');
            fid2 = fopen(filename2,'wt');
            fid3 = fopen(filename3,'wt');

            outputu = [real(u); imag(u)];
            fprintf(fid1,'%d    %d\n',outputu);
            outputv = [real(v); imag(v)];
            fprintf(fid2,'%d    %d\n',outputv);
            outputw = [real(w); imag(w)];
            fprintf(fid3,'%d    %d\n',outputw);

            fclose(fid3);
            fclose(fid2);
            fclose(fid1);
            scrivi = ['k=' dd ' fatto!'];
            disp(scrivi)
            clear u v w t U V W u1 v1 w1 t1
            toc
        end
    end
end
```

A.7 Collective random energy behaviour

The program `Collective_random_energy_behaviour` allow to sum randomly the perturbations. At each wave are associated two random numbers, the time to enter in the domain and the point of its life is entering. In this procedure the Fourier-transformed components $\hat{u}, \hat{v}, \hat{w}$ are used to calculate the collective energy distribution over the $(x - z)$ domain. Furthermore the collective energy in time is found.

```
%                       Collective_random_energy_behaviour


close all
clear all
format long
rr    = '30';
xx    = '50';
S     ={'sym' 'asym'};
A     = {'0' '45' '90' '45' '90' '0'};
kappa = [0.45 0.5 0.55 0.6 0.65 0.7 0.75 0.8 0.85 0.9 0.95 1 1.2 1.5 2,2.5 3...
         3.5 4 4.5 5 5.5 6 6.5 7 7.5 8 8.5 9 9.5 10 12 15 20 25 30 35 40 45 ...
         50 55 60 65 70 75 80 85 90 95 100 125 150 200 250 300 350 450 500];
Nonde = 408;
tend  = 50;
dt    = 0.0065;
t     = 0.00:dt:tend;
tt    = zeros(Nonde,1);
u     = zeros(Nonde,length(t));
v     = zeros(Nonde,length(t));
w     = zeros(Nonde,length(t));
ene   = zeros(1,length(t));
main_folder = 'D:\simulazioni\Interpolated_velocity_y0_linear';
% Load velocity files
n=1;
for i=1:2
    ss = S{i};
    for a=1:6
        gg = A{a};
        for m=17:50
            dd         = num2str(kappa(m));
            file_u     = ['\Re_' rr '_x_' xx '_' ss '_phi_' gg '_k_' dd '_u_int.txt'];
            file_v     = ['\Re_' rr '_x_' xx '_' ss '_phi_' gg '_k_' dd '_v_int.txt'];
            file_w     = ['\Re_' rr '_x_' xx '_' ss '_phi_' gg '_k_' dd '_w_int.txt'];
            folder_vel = ['\Re_' rr '_x_' xx '_' ss '_phi_' gg
                          '\Re_' rr '_x_' xx '_' ss '_phi_' gg '_k_' dd];
            filename1  = [main_folder folder_vel file_u];
            filename2  = [main_folder folder_vel file_v];
            filename3  = [main_folder folder_vel file_w];
            fid=fopen(filename1,'r');
            U=fscanf(fid,'%f',[2 length(t)]);
            fclose(fid);
            u(n,:)=U(1)+1i*U(2);

            fid=fopen(filename2,'r');
            V=fscanf(fid,'%f',[2 length(t)]);
            fclose(fid);
            v(n,:)=V(1)+1i*V(2);
```

```
            fid=fopen(filename3,'r');
            W=fscanf(fid,'%f',[2 length(t)]);
            fclose(fid);
            w(n,:)=(W(1)+1i*W(2))*((a<4)-(a>=4));

            tt(n)=length(U);
            n = n+1;
        end
    end
end
% Random vector
R = ceil(rand(Nonde,1).*tt/1.5)+1;
R(1:50:Nonde) = 0;

c = 1;
% Collective wave energy
for ab=1:c:length(t);
    eneU = 0;
    eneV = 0;
    eneW = 0;
    tic
    for n=1:Nonde
        if(R(n)<ab)
            IT   = 1 + mod(ab+tt(n)-R(n),tt(n));
            if (IT==1 && ab~=1)
                R(n)=ab+ceil(rand(1,1)*tt(n)/3);
            else
            eneU = eneU + u(n,IT);
            eneV = eneV + v(n,IT);
            eneW = eneW + w(n,IT);
        end
    end
    ene(ab) = sqrt(abs(eneU)^2 + abs(eneV)^2 + abs(eneW)^2);
end
figura = plot(t(1:c:ab),ene(1:c:ab)/ene(1));
nomefiguraM   = ['Re_' rr '_x_' xx '_energia.m'];
nomefiguraEPS = ['Re_' rr '_x_' xx '_energia.eps'];
saveas(figura,nomefiguraM)
saveas(figura,nomefiguraEPS)

nomeEnergy = ['Re_' rr '_x_' xx '_random_energy.txt'];
fid        = fopen(nomeEnergy,'w');
outpute    = [t(1:c:ab); ene(1:c:ab)];
fprintf(fid,'%d    %d\n',outpute);
fclose(fid);
```

Bibliography

[1] Belan, M., Tordella, D. (2002). *Asymptotic expansions for two-dimensional symmetrical laminar wakes.* ZAMM, 82 (4), 219-234.

[2] Benney, D. J., Gustavsson, L. H. (1981). *A new mechanism for linear and non-linear hydrodynamic instability.* Stud. in Applied Math., 64 (3), 185-209.

[3] Bergstrom, L. (1993). *Evolution of laminar disturbances in pipe Poiseuille flow.* Eur. J. Mech. B/Fluids, 12 (6), 749-768.

[4] R. Betchov, W. O. Criminale, *Stability of parallel flows*, New York (1967) Academic Press.

[5] Bogacki, Przemyslaw; Shampine, Lawrence F. (1989), *A 3(2) pair of Runge-Kutta formulas*, Applied Mathematics Letters 2 (4): 321-325,

[6] Bun, Y., Criminale, W. O. (1994). *Early-period dynamics of an incompressible mixing layer.* J. Fluid Mech., 273, 31-82.

[7] Butler, K. M., Farrell, B. F. (1992). *Three-dimensional optimal perturbations in viscous shear flow.* Phys. Fluids A, 4 (8), 1637-1650.

[8] Blossey, P. N., Criminale, W. O. Fisher, L. S. (2007). *Initial-value Problems in Free Shear Flows.* Submitted to J. Fluid Mech.

[9] L. Campbell, W. Garnett, *The Life of J.C. Maxwell and a Selection from his Correspondence and Occasional Writing and a Sketch of his Contributions to Science*, London (1882)

[10] Criminale, W. O., Drazin, P. G. (1990). *The evolution of linearized perturbations of parallel shear flows.* Stud. in Applied Math., 83 (2), 123-157.

[11] Criminale, W. O., Long, B., Zhu, M. (1991). *General three-dimensional disturbances to inviscid Couette flow.* Stud. in Applied Math., 85 (3), 249-267.

[12] Criminale, W. O., Jackson, T. L., Lasseigne, D. G. (1995). *Towards enhancing and delaying disturbances in free shear flows.* J. Fluid Mech., 294, 283-300.

[13] Criminale, W. O., Jackson, T. L., Lasseigne, D. G., Joslin, R.D. (1997). *Perturbation dynamics in viscous channel flows.* J. Fluid Mech., 339, 55-75.

[14] Criminale, W. O. , Drazin, P. G. (2000). *The initial-value problem for a modeled boundary layer.* Phys. Fluids, 12 (2), 366-374.

[15] Falkovich, Gregory and Sreenivasan, Katepalli R. *Lessons from hydrodynamic turbulence, Physics Today*, vol. 59, no. 4, pages 43-49 (April 2006).[2]

[16] U. Frisch, *Turbulence: the legacy of A. N. Kolmogorov*, Cambridge University Press (1995).

[17] Gustavsson, L. H. (1991). *Energy growth of three-dimensional disturbances in plane Poiseuille flow.* J. Fluid Mech., 224, 241-260.

[18] P. Huerre, P. A. Monkewitz, (1990). *Local and global instabilities in spatially developing flows.* Ann. Rev. Fluid Mech., 22, 473-537.

[19] Hultgren, L. S. , Gustavsson, L. H. (1981). *Algebraic growth of disturbances in a laminar boundary layer.* Phys. Fluids, 24 (6), 1000-1004.

[20] L. S. Hultgren, A. K. Aggarwal, (1987). *Absolute instability of the Gaussian wake profile.* Phys. Fluids, 30 (11), 3383-3387.

[21] A. N. Kolmogorov *Dissipation of Energy in the Locally Isotropic Turbulence*, Proceedings of the USSR Academy of Sciences **32**: 16-18. (1941)

[22] Lasseigne, D. G., Joslin, R. D., Jackson, T. L. , Criminale, W. O. (1999). *The transient period for boundary layer disturbances.* J. Fluid Mech., 381, 89-119.

[23] G. E. Mattingly, W. O. Criminale, (1972). *The stability of an incompressible two-dimensional wake.* J. Fluid Mech., 51, 233-272.

[24] Orr, W. M'F. (1907 a). *The stability or instability of the steady motions of a perfect liquid and a viscous liquid.* Part I. Proc. R. Irish. Acad., 27, 9-68.

[25] Orr, W. M'F. (1907 b). *The stability or instability of the steady motions of a perfect liquid and a viscous liquid.* Part II. Proc. R. Irish. Acad., 27, 69-138.

[26] Rayleigh, Lord (1880). *On the stability or instability of certain fluid motions.* Proc. London Math. Soc., 11, 57-70. Also, Scientific Papers, 1, 474-487, 1899.

[27] Schmid, P. J. , Henningson, D. S. (1994). *Optimal energy density growth in Hagen-Poiseuille flow.* J. Fluid Mech., 277, 197-225.

[28] Schmid, P. J. (2007). *Nonmodal Stability Theory.* Ann. Rev. Fluid Mech., 39, 129-162.

[29] Shampine, Lawrence F.; Reichelt, Mark W. (1997), *The Matlab ODE Suite*, SIAM Journal on Scientific Computing 18 (1): 1-22,

[30] Sommerfeld, A. (1908). *Ein beitraz zur hydrodynamischen erklaerung der turbulenten fluessigkeitsbewegungen.* Proc. Fourth Inter. Congr. Matematicians, Rome, 116-124.

[31] Sommerfeld, A. (1949). *Partial Differential Equations in Physics.* Lectures in Theoretical Physics, Vol. 6, Academic Press.

[32] K. R. Sreenivasan and R. A. Antonia, *The phenomenology of small-scale turbulence*, Annu. Rev. Fluid Mech. **29**, 35–72 (1997).

[33] G. S. Triantafyllou, M. S. Triantafyllou, C. Chryssostomidis, (1986). *On the formation of vortex street behind stationary cylinders.* J. Fluid Mech., 170, 461-477.